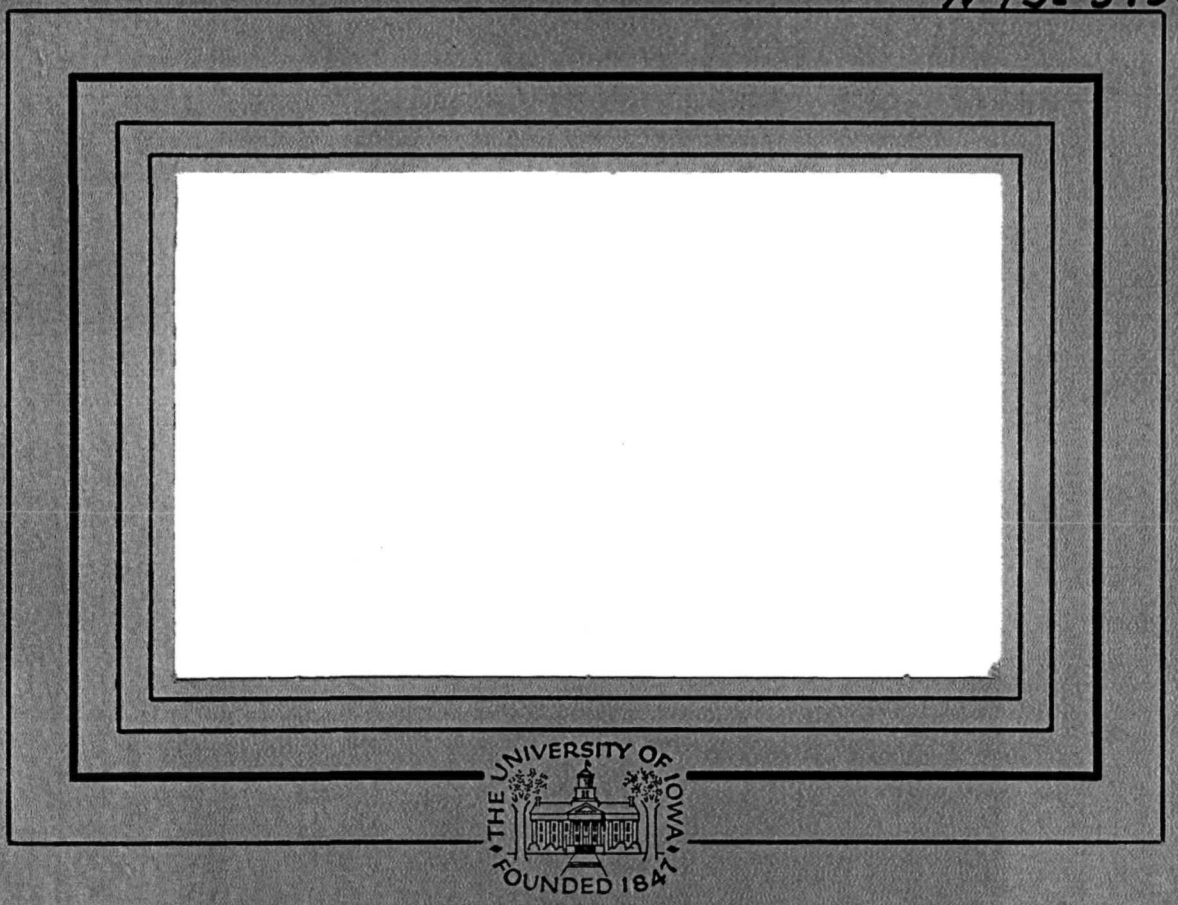

Department of Physics and Astronomy
THE UNIVERSITY OF IOWA
Iowa City, Iowa 52242

U. of Iowa 73-16

GENERATION AND PROPAGATION OF ELECTROMAGNETIC WAVES IN THE MAGNETOSPHERE

by

William W. L. Taylor

A thesis submitted in partial fulfillment of the
requirements for the degree of Doctor of Philosophy
in the Department of Physics and Astronomy
in the Graduate College of
The University of Iowa

May, 1973

Thesis supervisor: Assistant Professor Stanley D. Shawhan

ABSTRACT

Characteristics of broadband ELF, VLF, and LF emissions in the magnetosphere have been calculated assuming incoherent Cerenkov radiation from magnetospheric electrons with energies from 50 eV to 50 keV. Calculations were included to determine the ray paths of the emitted waves. A diffusive equilibrium model of the magnetosphere with an ionosphere, plasmapause, and a centered dipole magnetic field was used. Ray path calculations were done in three dimensions. Using simultaneous energetic electron and VLF data, comparisons were made between calculated and observed VLF hiss. VLF hiss is observed to have a sharp lower frequency cutoff near f_{LHR}, electric and magnetic field spectral densities as large as 1.4×10^{-8} V^2/m^2Hz and 9.6×10^{-26} Wb^2/m^4Hz, and wave normal angles a few degrees (~ 6) from the resonance cone. The calculated characteristics of VLF hiss include a sharp lower frequency cutoff near f_{LHR}, spectral densities of 5×10^{-8} V^2/m^2Hz and 1×10^{-30} Wb^2/m^4Hz, and wave normal angles very close ($\sim 10^{-6}$ to 10^{-3} degrees) to the resonance cone angle. Assuming a wave normal angle six degrees from the resonance cone angle, the calculated spectral densities are both two orders of magnitude below the observed spectral densities. It seems unlikely that VLF hiss is produced by incoherent Cerenkov radiation. The observed spectral shape of V-shaped VLF hiss is similar to that calculated from incoherent Cerenkov radiation. However, for V-shaped

VLF hiss to have its characteristic spectral shape, the emitting region must be small. Calculated spectral densities of incoherent Cerenkov radiation from this small region are orders of magnitude below observed spectral densities.

Observed characteristics of ELF hiss have been compared with incoherent Cerenkov and ray path calculations. ELF hiss is observed with spectral densities three and four orders of magnitude higher than calculated. Ray path calculations show that Cerenkov waves generated at high altitudes may not propagate to the low altitudes and over the wide range of latitudes where ELF hiss is observed.

The observed spectral shape of saucers is similar to that calculated for incoherent Cerenkov radiation. Calculated spectral densities are orders of magnitude below observed spectral densities.

Calculations assuming incoherent Cerenkov radiation of the spectral shape and spectral densities for fast hisslers agree with observations. However, to reach the ground where they have been observed, they must be generated at initial wave normal angles between 0.2° and 2.3° with respect to the magnetic field. Cerenkov radiation is generated at wave normal angles near the resonance cone. Fast hisslers have very short durations but incoherent Cerenkov radiation would be expected all along the path of the particles giving longer durations. Thus incoherent Cerenkov radiation seems to be ruled out for fast hisslers.

UHR (upper hybrid resonance) noise is observed to have wider spectral shapes and lower spectral densities than calculated from

incoherent Cerenkov radiation. Thermal effects may dominate at these frequencies and may have to be included in the theory.

Incoherent Cerenkov and cyclotron emission calculations were made in Jupiter's magnetosphere. A model of energetic electrons emitted and accelerated by Io rather than the electrons in the radiation belt were used in the calculation. The power levels calculated were fourteen orders of magnitude below the power observed in the decametric bursts which are associated with the orbital position of Io.

I. INTRODUCTION

The magnetosphere is a complex system of energetic particles, thermal plasma, and electromagnetic fields. It is clear that the sun is the main source of energy for magnetospheric dynamics and that the earth and its atmosphere act as the energy sink for the system. Understanding the process by which the energy is transferred from the sun to the magnetosphere; how the energy is distributed and passed between the magnetospheric energetic particles, thermal plasma, and electromagnetic fields; and how the energy is lost from the magnetosphere is one of the major objectives of the study of space physics. In particular, the study of the interactions between the energetic particles and the fields in the magnetosphere is thought to be the key to the complete understanding of the dynamics of the magnetosphere. There are a number of possible wave-particle interactions that may be of importance in the magnetosphere, and, to determine which dominate, quantitative studies of the theories must be done to compare their properties to magnetospheric data. It is just such a study which has been undertaken here to determine whether Cerenkov emission is responsible for the existence of ELF, VLF, and LF electromagnetic waves in the magnetosphere.

The Cerenkov mechanism has been a popular suggestion for explaining wave observations. Its popularity has been based on

some of its important characteristics:

(1) It is an incoherent mechanism so that it can occur regardless of plasma stability conditions.

(2) The emitted power comes primarily from the copius low-energy particles.

(3) The emission is broadband covering the frequency range of observed radio noise.

Previous calculations have had, at best, marginal success in explaining observations. The calculations to be presented here tend to indicate that incoherent Cerenkov emission may be responsible for UHR noise but is probably not responsible for VLF hiss, fast hisslers, and saucers.

In section II the theory of Cerenkov emission is reviewed, and a formula for the power emitted from a particle in a magnetoplasma including collisions is derived which, in the case of zero collision frequency, agrees with other derivations in the literature which were done for the case of no collisions. Section III describes ray tracing programs developed from Shawhan [1966, 1967] and the method of calculating electric and magnetic fields along the ray paths. Sections IV through VIII apply the results of sections II and III to particle and field data. Discussions of possible problems of the theory, including its possible inapplicability in some cases, and other effects and mechanisms which might be more successful in explaining some wave observations are given in section IX. Section X

gives results of Cerenkov calcultions done in the Jovian magnetosphere. Section XI summarizes the results of the Cerenkov and ray path calculations.

II. CERENKOV AND CYCLOTRON RADIATION IN A PLASMA

A. Cerenkov Radiation

A particle will produce Cerenkov radiation at a frequency f in passing through a medium whenever the velocity of the particle exceeds the phase velocity $v_p(f)$ of a wave in the medium. To see how a particle can produce Cerenkov radiation consider the case of a test electron moving in a straight line in a plasma. A moving electron will interact with the ambient electrons and ions of the plasma, primarily causing a momentary imbalance of the local charge neutrality by pushing electrons out of the vicinity and attracting ions to the vicinity of the moving electron. These interactions will therefore cause a momentary charge-separation electric field and a momentary current-induced magnetic field which results in a small electromagnetic pulse. The frequency components of the pulse which have phase velocities faster than the particle interfere destructively so that, at a distant point, the resultant field intensity is zero. The frequency components of the pulse which travel slower than the particle add coherently to produce a radiation field at an angle θ to the direction of the electron. θ is given by

$$\cos \theta = \frac{1}{\beta n} \quad ,$$

$$\beta = \frac{v}{c}$$

where n is the index of refraction of the medium at frequency f, v is the velocity of the particle, and c is the speed of light. Besides emitting Cerenkov radiation, a particle in a magnetic field $\vec{B}_o$ with a component of velocity perpendicular to $\vec{B}_o$ will radiate cyclotron radiation at an angle θ given by

$$\cos \theta = \frac{1 - s \frac{\omega}{\omega_{ge}}}{n\beta_2}$$

where

$s = \pm 1, \pm 2, \ldots ;$

$\omega = 2\pi f$, f = frequency;

ω_{ge} = electron gyrofrequency; and

$c\beta_2 = v_2$ = component of velocity parallel to $\vec{B}_o$.

B. Theoretical Treatments of Cerenkov Radiation in a Magnetoplasma

The two types of calculations that have been used to analyze the radiation from a particle gyrating in a magnetoplasma are the Hamiltonian method and the Fourier transform method. In the Hamiltonian approach the vector potential is expanded in a Fourier

series, which transforms a complicated set of partial differential equations for the vector potential into a system of ordinary differential equations for the coefficients of the series. Eidman [1958, 1959], Liemohn [1965], and Trulsen and Fejer [1970] used this method to calculate Cerenkov and cyclotron power in the absence of collisions.

In the Fourier transform method the electric field is transformed assuming an infinite series of plane waves. This procedure allows expansion of two time-dependent factors in a series of Bessel functions which reduces the problem to an integral of a series of Bessel functions. Mansfield [1967], McKenzie [1967], Melrose [1968], and H. C. Ko [private communication, 1972] have used this method to derive an expression for power in a cold, collisionless magnetoplasma. Trulsen [1971] has extended this method to include thermal effects through a temperature-dependent dielectric tensor. The resulting expressions from both approaches are in agreement. The derivation outlined here follows Mansfield's but includes the effects of collisions and corrects an error in one of Mansfield's symmetry relations.

The power radiated by an electron in moving through a plasma can be calculated by equating it to the work per unit time done on the particle by the charge-separation electric field. If q is the charge, $\vec{F}$ is the force, $\vec{v}$ is the velocity of the electron, and $\vec{E}$ is the electric field at the electron,

$$\vec{F} = q\vec{E} \quad ,$$

$$P = \vec{F} \cdot \vec{v}_q$$

$$= \vec{E} \cdot \vec{v}_q q \quad , \tag{1}$$

or, in terms of the current $\vec{J}$ $(= \vec{v}_q q)$,

$$P = \vec{E} \cdot \vec{J} \quad .$$

Equation (1) will be evaluated to determine the power emitted as Cerenkov radiation.

To determine graphically if Cerenkov radiation is possible for a set of plasma parameters and particle energies, the index of refraction surface may be used. The index of refraction surface is the locus of the tip of a vector $\vec{n} = (c/\omega)\vec{k}$, where $\vec{k}$ is the wave normal vector. The surface is longitudinally (rotationally) symmetric about the static magnetic field $\vec{B}_o$ and so is usually represented in two dimensions. Figure 1 shows a representative index of refraction surface and the procedure for using it to determine the existence of Cerenkov emission for a particle with a given velocity parallel to the static magnetic field. On the index of refraction surface for a frequency f a line is drawn perpendicular to $\vec{B}_o$ at a distance $1/\beta_2$ above the origin, where $c\beta_2$ is the velocity of the particle along $\vec{B}_o$. If the curves intersect, the Cerenkov condition is satisfied and the particle will radiate. For Figure 1 it is easiest to see the details in the schematic representation. In this particular

case the component of n along $\vec{B}_o$ does have a local maximum at $\theta = 0$ (as shown in the logarithmic representation). Consequently waves with four different wave normal angles will be radiated by that particle. A qualitative characteristic of Cerenkov radiation in the magnetosphere is that it is generated with wave normal angles close to the resonance cone angle where the index of refraction can exceed the longitudinal index of refraction for several orders of magnitude.

In a collisionless, cold plasma there are no dissipative forces, and the index of refraction approaches infinity as θ approaches the angle called the resonance cone angle. That means that a particle with a very small energy, even thermal energy, could Cerenkov radiate. As will be shown later, for small velocities the energy radiated from an electron is proportional to $1/v$, so to keep the energy radiated finite, as it must be, a limiting process is included in the theory. Limiting processes which might be evoked are:

(1) energy limits (a particle may not radiate more energy than it has) and

(2) index of refraction limits (by collisions or thermal effects).

In the derivation to follow, collisions have been assumed to be the limiting process. Collisions are introduced into the formalism through a phenomenological collision frequency.

C. Derivation of Cerenkov and Cyclotron Radiation Formulas Including Collisions

The assumptions made in deriving the Cerenkov and cyclotron emission expression are the following:

(1) The plasma is cold, homogenous, non-permeable ($\mu = \mu_o$), and immersed in a homogenous and static magnetic field.

(2) The collision frequencies are much smaller than the wave frequencies of interest.

(3) The test charges and the electromagnetic waves they emit can be neglected in the description of the plasma.

(4) Collisions are included to limit the index of refraction.

(5) The energy emitted by the test particle is much less than its kinetic energy.

As Eq. (1) states, the power emitted from an electron is

$$P = \vec{E} \cdot \vec{v}_q q \quad .$$

The equation of motion including a collisional drag force is

$$q_j(\vec{E} + \vec{v}_j \times \vec{B}_o) = m_j \frac{\partial \vec{v}_j}{\partial t} + \omega_{cj} \vec{v}_j m_j$$

where q_j, m_j, $\vec{v}_j$, and ω_{cj} are the charge, mass, velocity, and collision frequency, respectively, of the jth specie, $\vec{E}$ is the electric field at the particle, and $\vec{B}_o$ is the static magnetic field. Using Maxwell's equations, a formula may be derived for the Fourier transform of the electric field

$$\vec{E}(\vec{k}, \omega) = \frac{-i}{\omega\epsilon_o} \vec{\vec{T}}^{-1}(\vec{k}, \omega) \cdot \vec{J}_q(\vec{k}, \omega) \quad . \tag{2}$$

Here $\vec{J}_q$ is the Fourier transform of the current due to the test charge, and $\overleftrightarrow{T}$ is a tensor which includes all of the properties of the plasma and $\vec{B}_o$. The determinant of $\overleftrightarrow{T}$ set equal to zero is the dispersion relation for waves in the plasma. To find the power the inverse Fourier transform of the electric field, as given in Eq. (2), dotted into the velocity must be evaluated:

$$P = q \left[\iint d\vec{k} d\omega e^{i(\omega t - \vec{k}\cdot\vec{v})} \vec{E}(\vec{k}, \omega) \right] \cdot \vec{v}_q(t) \quad . \tag{3}$$

To calculate $\vec{J}_q(\vec{k}, \omega)$ the test charge velocity is expanded in a set of J Bessel functions. The integral required to Fourier transform $\vec{J}_q(\vec{r}, t)$ to $\vec{J}_q(\vec{k}, \omega)$ has a delta function in frequency as a factor,

$$\delta(s\ \omega_{ge} + n\omega \cos\theta\ \beta_2 - \omega)$$

where

s is the order of the Bessel function,

ω_{ge} is the gyrofrequency of the test electron,

n is the index of refraction,

ω is the wave frequency,

θ is the wave normal angle $= < (\vec{B}_o, \vec{k})$, and

$c\beta_2$ is the velocity of the particle along $\vec{B}_o$.

The integration over frequency results in a non-zero power only when $\vec{J}_q$ is non zero or when

$$s\ \omega_{ge} + n\omega \cos\ \theta\ \beta_2 - \omega = 0$$

or

$$\cos\ \theta = \frac{1 - s\ \frac{\omega_{ge}}{\omega}}{n\beta_2} \quad . \tag{4}$$

Notice that for $s = 0$, $\cos\ \theta = 1/n\beta_2$, which is the Cerenkov condition. The other s's are identified with cyclotron emission: $s > 0$ being normal cyclotron emission and $s < 0$ being anomalous cyclotron emission. The time-dependent factor in Eq. (3) is also expanded in a series of J Bessel functions, and the orthogonality of Bessel functions is used to convert the product of two series of J Bessel functions to a series of products of J Bessel functions. The integral over $\vec{k}$ in terms of J_s's may be converted to one over $\vec{n}$ and integrated by contour integration to an expression containing products of J's and $H^{(1)}$'s $\left[H_s^{(1)} = J_s + iY_s\right]$, where J_s and Y_s are the Bessel functions of the first and second kind of order s.

At this point in his derivation Mansfield made an error in the symmetry relations {Eqs. (33) in Mansfield [1967]} which allowed him to incorrectly discard two terms. The correct symmetry relation for

the complex calculation including collisions causes the imaginary parts to cancel in the frequency integral. Making the correction, the final expression for the power spectral density is

$$\frac{dP}{df} = \mathrm{Re} \sum_{j=1}^{2} \left| \frac{-\pi q^2 (-1)^j f}{\epsilon_o \epsilon_1 c^3 \beta_2 \left| n_1^2 - n_2^2 \right|} \sum_{s=-\infty}^{\infty} \left(v_1^2 J_s' H_s' T_{11} \right.\right.$$

$$+ v_1^2 \frac{s^2}{L_s^2} J_s H_s^{(1)} T_{22} + v_2^2 J_s H_s^{(1)} T_{33} + 2v_1^2 \frac{s}{L_s} J_s H_s^{(1)\prime} T_{12}$$

$$\left.\left. + 2v_1 v_2 J_s H_s^{(1)\prime} T_{13} + 2v_1 v_2 \frac{s}{L_s} J_s H_s^{(1)} T_{23} \right) \right|_{n=n_j} \qquad (5)$$

where

f is the frequency of the emitted wave = $\omega/2\pi$,

ϵ_o is the permittivity constant,

c is the speed of light,

v_1 is the component of the particle velocity perpendicular to $\vec{B}_o$,

v_2 is the component of the particle velocity parallel to $\vec{B}_o$,

$\beta_1 = v_1/c$,

$\beta_2 = v_2/c$,

J_s is the Bessel function of order s,

$H_s^{(1)}$ is the first Hankel function of order s $\left(H_s^{(1)} = J_s + iY_s\right)$,

Y_s is the Neuman function of order s,

L_s is the argument of all of the Bessel functions (J, Y, H),

$$L_s = \frac{\omega}{\omega_{ge}} \beta_1 \, n \sin \theta_s,$$

primes mean the derivative with respect to the argument,

θ_s is the wave normal angle $[\theta_s = < (\vec{k}, \vec{B}_o)]$ defined by Eq. (4),

s is the mode number,

$$T_{11} = \epsilon_1\epsilon_3 - \epsilon_1 n^2 \sin^2 \theta_s - \epsilon_3 n^2 \cos^2 \theta_s \ ,$$

$$T_{22} = \epsilon_1\epsilon_3 - \epsilon_3 n^2 + (n^4 - \epsilon_1 n^2) \sin^2 \theta_s \ ,$$

$$T_{33} = \epsilon_1^2 - \epsilon_2^2 - \epsilon_1 n^2 + (n^4 - \epsilon_1 n^2) \cos^2 \theta_s \ ,$$

$$T_{12} = \epsilon_2 n^2 \sin^2 \theta_s - \epsilon_2\epsilon_3 \ ,$$

$$T_{13} = \epsilon_2 n^2 \sin \theta_s \cos \theta_s \ ,$$

$$T_{23} = (n^4 - \epsilon_1 n^2) \sin \theta_s \cos \theta_s \ ,$$

$$\epsilon_1 = 1 - \sum_j \frac{\omega_{pj}^2}{\omega^2 - \omega_{gj}^2} \ ,$$

$$\epsilon_2 = - \sum_j \frac{\Gamma_j \omega_{gj} \omega_{pj}^2}{\omega\left(\omega^2 - \omega_{gj}^2\right)} ,$$

$$\epsilon_3 = 1 - \sum_j \frac{\omega_{pj}^2}{\omega^2} ,$$

Γ_j is the sign of the jth specie,

$$\omega_{pj}^2 = \frac{n_j q_j^2 \left(\omega^2 - i\omega_{cj}\omega\right)}{\epsilon_o m_j \left(\omega^2 + \omega_{cj}^2\right)} ,$$

$$\Gamma_j \omega_{gj} = \frac{q_j B_o \left(\omega^2 - i\omega_{cj}\omega\right)}{m_j \left(\omega^2 + \omega_{ij}^2\right)} ,$$

$i = \sqrt{-1}$,

Re means to take the real part of,

$\Big|\quad\Big|_{n=n_j}$ means to evaluate the expression inside the bars for a particular index of refraction n_j,

$$n_{1,2}^2 = \left[-B_n \pm \left(B_n^2 - 4C_n\epsilon_1\right)^{\frac{1}{2}}\right] / 2\epsilon_1 ,$$

$$B_n = \left(\frac{1 - s\,\frac{\omega_{ge}}{\omega}}{\beta_2}\right)(\epsilon_3 - \epsilon_1) + \epsilon_2^2 - \epsilon_1^2 - \epsilon_1\epsilon_3 ,$$

$$C_n = \left(\frac{1 - s \frac{\omega_{ge}}{\omega}}{\beta_2} \right)^2 \left(\epsilon_1^2 - \epsilon_2^2 - \epsilon_1 \epsilon_3 \right) + \epsilon_3 \left(\epsilon_1^2 - \epsilon_2^2 \right) ,$$

ω_{cj} is the phenomenological collision frequency of the jth specie,

$$\omega_{ce} = \omega_{ee} + \omega_{ei} ,$$

$$\omega_{ci} = \omega_{ii} + \omega_{ij} + \omega_{ie} ,$$

where ω_{ee} and ω_{ii}, the self-collision frequencies, are given by Spitzer [1956]; ω_{ei}, the electron-ion collision frequency, and ω_{ij}, the ion-ion collision frequency, are given by Nicolet [1953]; and ω_{ie}, the ion-electron collision frequency, is given by Sachs [1965] in terms of ω_{ie}. Note that every quantity is complex except q, f, ω, ϵ_o, c, $\beta_{1,2}$, $v_{1,2}$, ω_{cj}, and s, and that this is due to the addition of collisions which adds an imaginary part to the plasma and gyrofrequencies. Mansfield's original calculations left out the T_{12} and the T_{13} terms for his expression for $s \neq 0$, but did lead to the correct expression for $s = 0$ (T_{11}, T_{33}, and T_{13} terms). McKenzie [1967], Melrose [1968], and Trulsen and Fejer [1970] have all published results which agree with Eq. (5) for the collisionless case. H. C. Ko [private communication, 1972] has also redone Mansfield's calculations and agrees with these results. For the details of the derivation the reader is referred to Mansfield [1967].

For s = 0 and small velocities, the power radiated by the T_{33} term dominates. It is proportional to 1/v and the others vary as v.

A program has been developed which calculates the power per unit volume emitted by a spectrum of energetic electrons at a frequency f for specified plasma parameters. Eq. (5) is evaluated for each of eighteen pitch angles, 2.5°, 7.5°, ..., 87.5°, for each energy included in the electron energy spectrum. The energy spectrum is approximated by specifying the equivalent number density of electrons in energy intervals centered on a finite number of energies. The program calculates the number density of the energetic electrons in each pitch angle segment $(\text{electrons/dV})_{E_i,\alpha_j}$, and multiplies it by the power emitted per particle per unit frequency (dP/df electrons) to get the power emitted per unit volume per unit frequency $(d^2P/dVdf)_{E_i,\alpha_j}$. The sum

$$\frac{d^2P}{dfdV} = \sum_{i,j} \frac{d^2P}{dfdV}_{E_i,\alpha_j}$$

is then performed. A representative wave normal angle θ [corresponding to the largest $(d^2P/dfdV)_{E_i,\alpha_j}$] is then chosen to represent the direction of the wave normal angle for $d^2P/dfdV$. (In general, the spread in θ values is $\ll 1°$.) Two cards are punched for input to the ray tracing program, each with one half of $d^2P/dfdV$ as the volume emissivity and with θ and -θ as wave normal angles. This means that the power is not assumed to be radiated in a cone, but in two

directions, corresponding to the intersection of the cone and the magnetic meridian plane.

III. RAY TRACING AND FIELD CALCULATION

A. Ray Tracing Routines

After the power is calculated from a spectrum of electrons it is desirable to determine the path the emitted power follows through the magnetosphere. Shawhan [1966, 1967] has developed a computer routine to do this calculation in the meridian plane. Using this routine as a basis four routines were written, including collisions in the ray tracing expressions and including a calculation of the collisional damping the wave experiences as it propagates. Two of the routines were for two spatial dimensions (r, θ; i.e., in the meridian plane) and two were for three spatial dimensions (r, θ, φ). The dependent variables in the two-dimensional routines were, in the first case, r, θ, and ψ where r is the radial distance from the center of the earth, θ is the colatitude, and ψ is the wave normal angle; and, in the second case, r, θ, ρ_r, and ρ_θ where ρ_r and ρ_θ are the components of the index of refraction in the r and θ directions. The dependent variables in the first three-dimensional routine were r, θ, φ, Δ, and ϵ where φ is the longitude, Δ is the angle between the radial direction and the vector $\vec{k}_m$ (the projection of the $\vec{k}$ vector in the meridian plane), and ϵ is the angle between $\vec{k}_m$ and $\vec{k}$. In the second the dependent variables were r, θ, φ, ρ_r, ρ_θ, and ρ_φ where ρ_φ is the component of the index of refraction in the φ direction.

All of the routines were checked by reproducing results of Kimura [1966] and by consistency checks. Validity checks will be discussed further in section IX. The versions using angles were considerably faster computationally because only one (two) angles in two (three) dimensions are necessary to completely specify the index of refraction. Two (three) components are required in the versions using the ρ's. In the over-determined routines (versions using ρ's) the index of refraction must be corrected at each integration step which decreases integration accuracy and hence decreases execution speed. Consequently the routines using angles were used for all of the results given here.

B. Electric and Magnetic Field Calculations

To compare the theory to data it is often desirable to calculate spectral densities of fields from the spectral density of power. Mosier and Gurnett [1971] have already made the conversion from fields to powers in their Eqs. (1), (2), and (4). They are as follows:

$$E_x = e_x \cos(-\omega t) \quad , \qquad B_x = b_x \sin(-\omega t) \quad ,$$

$$E_y = e_y \sin(-\omega t) \quad , \qquad B_y = b_y \cos(-\omega t) \quad ,$$

$$E_z = e_z \cos(-\omega t) \quad , \qquad B_z = b_z \sin(-\omega t) \quad ,$$

where

$$e_x = E_o \quad , \qquad b_x = \frac{n \cos\theta}{c} \frac{\epsilon_2}{s - n^2} E_o \quad ,$$

$$e_y = \frac{-\epsilon_2}{\epsilon_1 - n^2} E_o \quad , \qquad b_y = \frac{n \cos\theta}{c} \frac{\epsilon_3}{\epsilon_3 - n^2 \sin^2\theta} E_o \quad ,$$

$$e_z = - \frac{n^2 \cos\theta \sin\theta}{\epsilon_3 - n^2 \sin^2\theta} E_o \quad , \qquad b_z = - \frac{n \sin\theta}{c} \frac{\epsilon_2}{\epsilon_1 - n^2} E_o \quad ,$$

$$E_o = \langle s_z \rangle \frac{2\mu_o c}{n \cos\theta} \frac{1}{\dfrac{\epsilon_3}{\epsilon_3 - n^2 \sin^2\theta} + \dfrac{\epsilon_2^2}{\left(\epsilon_1 - n^2\right)^2}} \quad ,$$

$\langle s_z \rangle$ is the z component of the time averaged Poynting flux,

$\langle s_z \rangle = s \cos\varphi$, $\varphi = < (\vec{B}_o, \vec{v}_g) = \theta + \alpha$, and

$$\alpha = < (\vec{n}, \vec{v}_g) = \tan^{-1} \left(- \frac{1}{n} \frac{dn}{d\theta} \right) \quad , \qquad \theta = < (\vec{k}, \vec{B}_o) \quad .$$

The geomagnetic field $\vec{B}_o$ is in the z-direction and the wave normal angle for the two-dimensional program is in the x-z plane. The calculation of the electric and magnetic field components is done point-by-point in the ray path calculation.

IV. VLF HISS

A. Observations

VLF hiss has been described by a number of investigators [Helliwell, 1965; Gurnett, 1966; Jørgensen, 1966; McEwen and Barrington, 1967; Laaspere et al., 1971; Gurnett and Frank, 1972; and others]. Laaspere et al. [1971], Barrington et al. [1971], and D. A. Gurnett [private communication, 1972] characterize the spectral shape of VLF hiss in low-altitude satellite observations as having a sharp lower-frequency cutoff, the largest spectral density just above the lower-frequency cutoff, and an intensity which is slowly monotonically decreasing with increasing frequency above the maximum spectral density. The lower-frequency cutoff is generally thought to be the local lower hybrid resonance frequency where downgoing waves are reflected so that lower frequency waves propagating down are not observed. Jørgensen [1968] reported low-altitude satellite observations of VLF hiss which seemed to have a maximum near 10 kHz with gradually decreasing fluxes above and below 10 kHz. However, he drew this conclusion from 26 two-point spectra, all of which could also be fit with the spectra found by Laaspere et al. [1971], Barrington et al. [1971], and D. A. Gurnett [private communication, 1972]. The lower-frequency cutoff of VLF hiss is usually 2 to 6 kHz with upper-frequency cutoffs as high as 540 kHz.

Figure 2 shows an Injun 5 VLF hiss spectrogram taken from Mosier and Gurnett [1972].

A low-altitude satellite usually observes VLF hiss for only a matter of minutes, but this variation is considered to be spatial rather than temporal since observations of VLF hiss have been made on consecutive orbits ninety minutes apart at the same location, indicating durations at least occasionally of a few hours.

Gurnett [1966], using Injun 3 data, found that the spatial occurrence of 5.5—7.0 kHz VLF hiss $\geq 3 \times 10^{-10}$ γ^2/Hz was predominately from 12 to 24 hours magnetic local time and 7° wide in invariant latitude, with the latitude of peak occurrence being about 77° at 14 hours decreasing to 70° at 22 hours.

Gurnett and Frank [1972], using Injun 5 data, found an association between VLF hiss in the auroral zone and high fluxes of low-energy electrons. They found the associated VLF hiss and electrons on field lines connected to the dayside polar cusp and to the downstream magnetosheath and distant plasma sheet which are the topological extensions of the polar cusp into the magnetotail. Gurnett and Frank also found the VLF hiss to be generally propagating down the geomagnetic field lines with power fluxes occasionally as large as 10^{-11}—10^{-12} w/m^{2}Hz at 2.5 kHz. (See also Mosier and Gurnett [1972].) The electrons associated with these VLF hiss events had energies on the order of 100 ev to several kev and fluxes of about 10^9 electrons (cm^2 sec ster)$^{-1}$. In addition, a 'threshold' effect was found

between the VLF and electron fluxes. For electron fluxes below 10^4—10^5 electrons $(cm^2 \text{ sec ster})^{-1}$ at 100 ev little or no VLF hiss was observed, but above this 'threshold' Gurnett and Frank found that VLF hiss was essentially always observed. However, VLF hiss was found to be not necessarily proportional to the low-energy electron flux. In one case (Figure 4 [Gurnett and Frank, 1972]) $dj/dE(160 \leq E \leq 280 \text{ ev})$ increased one and one-half orders of magnitude, but dE^2/df ($f = 7.35$ kHz) increased three and one-half orders of magnitude.

Since VLF hiss is predominately downgoing, Gurnett and Frank [1972] suggest that the generation region is above the satellite, and have made a rough estimate of the altitude of the generation region to be about 5000 to 10,000 km.

Laaspere et al. [1971] have reported an estimate of peak flux for VLF hiss of 6×10^{-12} w/m^2Hz at 'audio' frequencies from OGO-6 data. This agrees with the measurements of Gurnett and Frank [1971] even though OGO-6 had only an electric field detector. To calculate power fluxes from electric fields Laaspere et al. [1971] assumed that the propagation was longitudinal, that the wave normal angle was zero, and that the index of refraction was unity.

With Alouette 2 electric-field data Barrington et al. [1971] reported an average signal intensity of 2×10^{-11} w/m^2Hz at 10 kHz assuming an index of refraction of 10 and an average over a range of wave normal angles.

B. Mechanisms for Producing VLF Hiss

Various mechanisms have been suggested for the generation of VLF hiss. The Cerenkov mechanism has been considered by Ellis [1957, 1959, 1960], Dowden [1960], McKenzie [1963, 1967], Liemohn [1965], Seshadri and Tuan [1965], Gershman and Trakhtengerts [1966], Jørgensen [1968], Hartz [1970], Trulsen and Fejer [1970], Lim and Laaspere [1972], and James [1973]. Another popular mechanism suggested for VLF hiss is cyclotron emission, described by Ellis [1959], MacArthur [1959], Murcray and Pope [1960, 1961], Santirocco [1960], Gintsburg [1961], Gershman and Trakhtengerts [1966], Trulsen and Fejer [1970], and Trulsen [1971]. Another mechanism suggested is a plasma instability, the traveling wave tube mechanism of Gallet and Helliwell [1959] and Dowden [1962].

C. The Cerenkov Calculations of Jørgensen and Lim and Laaspere

Of the Cerenkov calculations, Jørgensen's [1968] and Lim and Laaspere's [1972] are the easiest to compare to VLF hiss data. Jørgensen used Mansfield's [1967] theoretical results for the power emitted by a particle gyrating in a magnetoplasma and calculated a VLF hiss spectrum he claimed would be observable in the lower ionosphere. Jørgensen used an intense but reasonable electron spectrum determined by Evans [1966] for energies above 1 kev shown in Figure 3 and he assumed an isotropic pitch angle distribution. He also assumed the power produced to be independent of the pitch angle of the

energetic electrons. He chose the field line corresponding to 70° invariant latitude (L = 8.5) and assumed perfect guiding of the emitted waves. The guiding allowed him to add all the power produced in a flux tube. He chose the upper limit for power production to be 26,000 km. Jørgensen justified his assumption of perfect guiding on the basis of ducting. Jørgensen's results are shown in Figure 4. He calculated a maximum spectral density of about 10^{-14} w/m^2Hz at about 10 kHz. This is two to three orders of magnitude less than the most intense VLF hiss spectral densities determined by Gurnett and Frank [1972] and Mosier and Gurnett [1972] using Injun 5 data, and two orders of magnitude below the maximum VLF intensity measured with Injun 3 [Gurnett, 1966]. In the same paper Jørgensen reported OGO-2 observations of VLF hiss. The maximum spectral density was 4.4×10^{-12} w/m^2Hz at 18.5 kHz with a typical average spectral density of 10^{-14}—10^{-15} w/m^2Hz. The spectral densities reported were at frequencies from 2.3 to 88 kHz.

However, Jørgensen's [1968] OGO-2 power spectral densities were obtained from the observed magnetic spectral densities using a formula from Helliwell [1965] which is applicable only for longitudinal propagation (wave normal angle = 0°). As shown qualitatively in section II, for the Cerenkov and cyclotron mechanisms the wave normal angle is considerably different from zero and is near the resonance cone angle where the index of refraction n is large. This large n allows the phase velocity of the wave to be comparable to

the velocity of the radiating particle. This condition is necessary for most wave-particle interactions. It is likely that the emitted wave normal angle of the VLF hiss wave is close to the resonance cone no matter what the mechanism. Ray path calculations of waves emitted above satellite altitudes with wave normal angles near the resonance cone show that wave normal angles stay near the resonance cone. These paths are shown in Figure 5. Therefore it seems that Jørgensen's conversion from magnetic fields to powers is not justified. If Jørgensen's observations were of waves with non-zero wave normal angles, the power calculated was too low since magnetic fields get smaller as the wave normal angle gets close to the resonance cone angle.

Also, a second assumption that Jørgensen made does not seem to be justified. He assumed that the waves were perfectly guided from 26,000 km to satellite altitudes. However, ray tracings of Cerenkov generated rays indicate that rays with frequencies above 2 kHz are dispersed over a larger latitudinal and longitudinal extent than the particle precipitation region. Consequently, this dispersion leads to a power loss factor up to a factor of 100. Representative dispersed ray paths for 2 and 10 kHz from 6250 and 8750 km are shown in Figure 6.

The most recent calculations of VLF hiss, by Lim and Laaspere [1972], have made improvements over the calculations by Jørgensen but still fall short of explaining the maximum VLF hiss intensities

observed. They also used Mansfield's formula for Cerenkov power. They made the proper corrections and recognized the problem of infinite power radiated from low-energy particles at resonances, and limited the index of refraction to 400. The electron spectrum chosen by Lim and Laaspere was similar to Westerlund's [1968] but softer. (See Figure 3.) Isotropy was also assumed. Calculations were made at frequencies from 4 to 1180 kHz and, as in Jørgensen [1968], they added all the power in a flux tube. They chose an invariant latitude of 78°. Their calculated hiss spectrum is also shown in Figure 4. Two orders of magnitude still separate the maximum observed Injun 5 and Lim and Laaspere's calculated VLF fluxes.

To avoid the power infinity Lim and Laaspere placed a limit of 400 on the index of refraction, corresponding to the condition that the phase velocity of the emitted wave was twice the thermal velocity of the background electrons for their assumed electron temperature of 5000 °K. However, Stix [1962] and Kennel and Petschek [1966] give the analog of Laudau damping for oblique waves to be when $k_{\|}v_{\|} = \omega$. Physically the guiding centers of the plasma particles are confined to move along the magnetic field, so that the interaction is between the projection of the phase fronts onto the direction of the geomagnetic field, $\vec{B}_o$, and the resonant particles which are constrained to first order motion along $\vec{B}_o$. For example, at an altitude of 10,000 km and a geomagnetic latitude of 70° the resonance cone angle at 4 kHz is about 80°. An $n_{\|}$ of 400 corresponds to an n of about

2200. In other words, Lim and Laaspere should have placed the limit on $n_{\parallel}$ rather than on n. Restricting $n_{\parallel}$ could make an order-of-magnitude increase in their power calculations which would be in agreement with the upper limit calculation presented in the next part.

Limiting n rather than $n_{\parallel}$ probably increased Lim and Laaspere's frequency of peak power. Slightly above f_{LHR} the resonance cone angle is close to 90°, and although n may be very large, $n_{\parallel}$ is small, and the power at these frequencies was not included by Lim and Laaspere. Since the region of resonance, and thus high Cerenkov power, in the frequency range is $f_{LHR} < f < \min (f_{ge}, f_{pe})$, Lim and Laaspere underestimated the power at the lower frequencies.

The spectral shapes of VLF hiss calculated by Jørgensen [1968] and Lim and Laaspere [1972] were dissimilar. Jørgensen's was peaked at 10 kHz, with a gently decreasing spectral density above and below 10 kHz. This spectrum was consistent with the VLF hiss spectrum he deduced from twenty-six observations of spectral density at two frequencies from the set [2.3, 5.1, 8.4, 11, 18.5, 40, 60, 88 kHz]. It is not consistent with the VLF hiss spectra observed by Laaspere et al. [1971], Barrington [1971], and D. A. Gurnett [private communication, 1972]. Lim and Laaspere's spectrum had a maximum at 70 kHz, gently decreasing below 70 kHz and dropping off rapidly above 70 kHz. This spectrum is considerably different from any VLF hiss spectrum thought to be typical.

D. Cerenkov Production of VLF Hiss

1. Upper Limit Calculation

Low-energy electrons which have large fluxes in the auroral zone will emit significant amounts of energy in the Cerenkov mode only for frequencies which may propagate with a large index of refraction. The frequencies for which this condition holds in the VLF hiss range is $f_{LHR} < f < \min (f_{pe}, f_{ge})$. It is in this frequency range that calculations of incoherent Cerenkov noise similar in spirit to Jørgensen's [1968] and Lim and Laaspere's [1972] have been made. An even more intense electron spectrum measured with an electrostatic analyzer on the Twins I rocket in an aurora, from Westerlund [1968], was used. (See Figure 3.) This spectrum is somewhat more intense than the ones measured by Injun 5 LEPEDEA's [Ackerson and Frank, 1972] during an $\sim 3 \times 10^{-11}$ w/m^{2}Hz VLF hiss event described by Mosier and Gurnett [1972]. The maximum electron flux is 1 to 2 orders of magnitude larger than the one used by Jørgensen and the spectrum is extended down to about 45 ev. Westerlund's spectrum was the most intense that could be found in the literature. Isotropy was assumed, and power was calculated in each of eighteen pitch angle segments. The index of refraction was limited by including collisions and by requiring that the phase velocity of the emitted wave along the magnetic field direction be higher than the thermal velocity of the background electrons. For an electron temperature of 5000 °K this limits $n_{\parallel}$ to about 600. This procedure avoids the problem of infinite

calculated power. The background plasma was represented by an electron-three ion diffusive equilibrium model with an ionosphere having a maximum electron density of 10^6 cm^{-3} at 150 km altitude and a plasmapause at L = 4. Two altitude profiles from the model are shown in Figure 7 for magnetic latitudes of 0° and 70°. A centered dipole was used as a model for the earth's magnetic field. The calculations were made at 70° invariant latitude and all the power in a 1 m^2 flux tube was added assuming perfect guiding. Upper-altitude limits were chosen to be 26,000 km (as Jørgensen [1968]) and 48,000 km (the equator). Account was taken of the flux tube expansion. The results are shown in Figures 4 and 8. Figure 8 shows power produced in 2000 km altitude segments for different frequencies and Figure 4 shows the power summed along the field line. The power peak of about 7×10^{-13} w/m^2Hz at 10 kHz is nearly as large as the power estimated at 8.8 kHz from Injun 3 data by Gurnett [1966]. The calculated power at 3 kHz, $2—3.5 \times 10^{-13}$ w/m^2Hz, is two orders of magnitude below the power of about 3×10^{-11} w/m^2Hz measured by Mosier and Gurnett [1972]. As with previous calculations, the calculated spectrum has a maximum at the wrong frequency and has an incorrect lower-frequency cutoff.

This type of calculation gives only a rough estimate of the maximum incoherent Cerenkov power which might be observed at satellite altitudes. A more accurate calculation would determine the exact ray paths of the waves after they are emitted by the Cerenkov mechanism.

The waves are approximately guided by the earth's magnetic field but do diverge in latitude and longitude. The energetic electron spectra used should be that measured at the altitude of generation and it is not expected to be constant as a function of altitude. The attenuation of the waves as they propagate from the generation region to the observation region should be included. Experimentally, wave power is calculated from one or more field components, whereas in a theoretical calculation the fields can be determined exactly from the power, wave normal angle, and plasma parameters. It seems reasonable then to compare the directly measured quantities, fields, with the calculated fields rather than a derived quantity, power, with calculated power.

2. Detailed Calculation

In order to make a more accurate estimate of what VLF hiss intensity a low-altitude satellite would observe from electrons radiating in the Cerenkov mode, a more sophisticated calculation has been performed. Cerenkov power was calculated from an electron spectrum measured during the same VLF hiss event that was characterized as among the most intense observed with Injun 5, shown in Figure 2. Mosier and Gurnett [1972] reported VLF hiss observations and Ackerson and Frank [1972] reported plasma measurements during the same auroral-VLF hiss-electron precipitation event on December 21, 1968. The energetic electron spectrum reported was used to calculate Cerenkov power at altitudes up to 10,000 km, which Gurnett and Frank [1972]

suggest might be the maximum altitude of primary auroral electron acceleration. The three-dimensional ray tracing program calculated the ray paths from the generation region to an altitude of 2500 km, the approximate satellite altitude.

The locus of points where the ray paths crossed 2500 km was approximately circular. The width of the precipitation region was estimated from Plate 2 of Ackerson and Frank to be about 1.8° of arc at the 2500 km altitude level. The power loss factor due to collisional damping and to spreading of the wave energy to a region greater than that of precipitation can be estimated to be [(width of wave illumination region)/(width of precipitation region)]^2 x [collisional loss]. The power expected at satellite altitude is then

$$\frac{dP}{df} = \sum_i \left(\frac{d^2P}{dfdV}\right)_i V_i(\text{loss})_i$$

where $d^2P/dfdV$ is the power spectral density per unit volume emitted by the energetic electrons radiating in the Cerenkov mode and V is the volume of the emitting region, the volume of the ith section of the flux tube with one m^2 cross sectional area. The summation was done in sections from 2500 km to 10,000 km, with $d^2P/dfdV$, V, and loss calculated for each section. Similar calculations were made for dE^2/df and dB^2/df.

Figure 9 shows the spectral densities of the power and of the electric and magnetic fields that would be expected during the

December 21, 1968 event due to Cerenkov radiation. Note that the power and fields are very much smaller for frequencies below the local f_{LHR}. Mosier and Gurnett report that the maximum intensity of the VLF hiss occurred at 1h 52m 47s and the broadband (0.3 to 10 kHz) electric and magnetic field strengths were 8.4×10^{-3} V/m and 22 mγ, respectively. From these facts and the facts that the cosine correlation $\langle \cos \varphi \rangle$ was measured to be about 0.5 and the bandwidth was estimated to be 5 kHz, they found the lower limit of the VLF hiss power flux to be 1.5×10^{-11} w/m^2Hz. Converting the measured fields to spectral densities assuming a 5 kHz bandwidth gives

$$\frac{dE^2}{df} = 1.4 \times 10^{-8} \ V^2/m^2Hz$$

$$\frac{dB^2}{df} = 9.6 \times 10^{-26} \ Wb^2/m^4Hz \quad .$$

Comparing these spectral densities to Figure 9 it is seen that the calculated spectral density of the electric field is the same order of magnitude as the measured one but a little larger, and the calculated spectral densities of the power and magnetic field are considerably below the measured fields by factors of $10^{-2.5}$ and 10^{-5}, respectively. A combination of two possible effects may account for this discrepancy.

The first effect involves the dependence of electric and magnetic field amplitudes upon wave normal angle. For a constant power, as the wave normal angle of a wave approaches the resonance cone angle, the electric field of the wave increases and the magnetic field decreases. As mentioned above, the wave normal angle of a wave generated by the Cerenkov mechanism is generally very close to the resonance cone angle at generation and during propagation. The dependence of electric and magnetic field spectral densities upon wave normal angle is shown in Figure 10. Figure 10 was calculated for the 2500 km altitude level of a 2 kHz wave generated by the Cerenkov mechanism at 6250 km altitude. There is a difference of a factor of 10^3 in the spectral densities between waves with wave normal angles characteristic of Cerenkov production ($\sim 10^{-6}$ degrees from the resonance cone) and waves with wave normal angles only one degree from the resonance cone angle. There is some dispersion in initial wave normal angles due to the fact that particles with different energies and pitch angles radiate at different wave normal angles. For the situation here, however, this dispersion is usually less than 0.1°. If, for some reason (perhaps irregularities in the background plasma or by thermal dispersion), some of the waves produced by the Cerenkov mechanism were to deviate by a degree or more from the resonance cone angle, the electric field spectral density would remain high (from the waves with undeviated wave normal angles) and the magnetic field spectral density would increase by a factor of about 10^3.

The improved calculation above gives an electric field spectral density about 3.5 times the observed one. Therefore only 28% of the waves need to have wave normal angles comparable to the ones calculated by the ray tracing program. If the other 72% have wave normal angles about a degree from the resonance cone angle, the magnetic field measured would be about 720 times the one predicted by the ray tracing program, or

$$\frac{dB^2}{df} = 7.2 \times 10^{-28} \text{ Wb}^2/\text{m}^4\text{Hz} \quad .$$

This spectral density is about two orders of magnitude below the observed magnetic field spectral density. Mosier and Gurnett [1971] have shown, however, that in the power calculation they perform the cosine correlation would be small in a case of wave normal angle dispersion for uncorrelated waves. Since the cosine correlation is typically near 0.5 for VLF hiss, there must be little wave normal angle dispersion.

The second effect which might account for a higher measured than calculated power density is the possible sensitivity of a magnetic loop to electric fields. D. A. Gurnett [personal communication, 1973] has made a rough calculation of the voltage ratio expected between the electric and magnetic components of a wave propagating in free space for an unshielded 1 meter loop at a frequency of 3 kHz. The ratio was determined to be about 10^{-5}. Since the

Injun 5 magnetic loop has 6 turns and has a diameter of 0.56 m, the relative sensitivity in free space from this calculation is perhaps an order of magnitude less or about 10^{-6}. However, the sensitivity would be greater for waves in a plasma near the resonance cone since the index of refraction would be larger as would the electric field. Using the same sample ray calculation as was used in Figure 10, the ratio of E to B was calculated and found to be 5.75×10^{11} m/s, a factor of 2×10^{3} larger than c, the ratio of E to B in free space. In Gurnett's calculation free space propagation was assumed and $E/B = c$ was used. A correction for the plasma then is to use $E/B = c \times 2 \times 10^{3}$ which changes the voltage ratio to $\sim 5 \times 10^{-2}$, still an insignificant correction.

An experimental determination of the sensitivity of the Injun 5 magnetic loop to electric fields was performed and it was determined that at 3 kHz a 130 mV/m electric field induced a signal in the magnetic loop equal to that produced by a magnetic field of 0.1 mγ, the approximate noise level in the loop. The intense VLF hiss event described above [Mosier and Gurnett, 1972] had an electric field of only 8.4 mV/m. It is unlikely, on the basis of this experiment, that magnetic field observations from Injun 5 are incorrect. It is concluded that the apparent magnetic field induced by the observed electric fields is below the magnetic receiver noise level and could not contribute to the observed magnetic field.

At the time of maximum measured VLF intensity the electric field spectrum of the VLF hiss in Figure 2 has a sharp lower cutoff

at about 1 kHz, which is similar to the spectrum in Figure 9. This lower cutoff is thought to be at the local f_{LHR}, so a small change in the model would reduce the calculated lower-frequency cutoff to agree with the data. The upper-frequency cutoff is not as sharp, with noise evident up to perhaps 7 kHz. If the dynamic range of the spectral analysis system is about 3 db, this agrees with the calculated electric field spectrum in Figure 9 which is down to 1/2 its maximum value at 7 kHz. This decrease in power for higher frequencies is due to the increased angular dispersion of the ray paths as the wave frequency increases. Even though more power is generated at higher frequencies the spreading of the power over larger areas more than compensates for the increased power, resulting in an observed spectrum peaked near the lower cutoff frequency. The magnetic field spectrum in Figure 2 appears flatter but still has upper- and lower-frequency cutoffs. The calculated magnetic field spectrum is also flatter, but it extends to at least 10 kHz.

Laaspere et al. [1971] estimate the 'audio' frequency power from an intense auroral hiss event to be of the order of 6×10^{-12} w/m^2Hz, which corresponds to an electric field spectral density of about 10^{-9} V^2/m^2Hz about 50 times lower than the maximum in Figure 9. Barrington et al. [1971] estimate an average signal intensity at 10 kHz of 2×10^{-13} w/m^2Hz, which corresponds to an electric field spectra density of about 3×10^{-11} V^2/m^2Hz. Jørgensen [1968] estimated a maximum power spectral density of 4.4×10^{-12} w/m^2Hz

corresponding to a magnetic field spectral density of about 10^{-25} Wb^2/m^4Hz, very close to the Injun 5 measurements of Mosier and Gurnett [1972]. These calculations and measurements of VLF hiss power and field densities are summarized in Table 1.

The E/B ratio calculated for the event shown in Figure 2 corresponds in the model to an index of refraction of about 8 and a wave normal angle about 6° from the resonance cone. Since the cosine correlation was found to be 0.5, the wave normal angle dispersion was at most a few degrees. If the wave normal angle of the Cerenkov waves as calculated here were actually 6° from the resonance cone, the electric field would be reduced and the magnetic field would be increased by 3 orders of magnitude. The calculated spectral densities in this case would be factors of about 350, 100, and 300 below the observed spectral densities for the electric field, the magnetic field, and the power, respectively. Even though the spectrums have the right shape, the fact that the calculated and observed spectral densities are so much different for VLF hiss seems to rule out incoherent Cerenkov radiation as the source of VLF hiss. Other possible source mechanisms are discussed in Section IX.

3. Cyclotron Modes

The contribution to VLF hiss by other incoherent modes ($s > 0$, cyclotron radiation and its harmonics, and $s < 0$, anomalous cyclotron radiation) was judged to be minor, at least for the most intense

lower frequencies. Figure 11 shows the power emitted from the electron spectrum used in the above calculation of VLF hiss at an altitude of 10,000 km and an invariant latitude of 70° for various modes. Except very near the plasma frequency, the cyclotron contribution is an order of magnitude below the Cerenkov power.

E. V-Shaped VLF Hiss

One form of VLF hiss that is observed in low-altitude satellites is V-shaped hiss, observed to be propagating down the field lines, in which the minimum frequency of the hiss first decreases and then increases in time, with a total width of 30 seconds or more and a minimum frequency of 1 kHz or more.((See Gurnett [1966], Gurnett et al. [1971], and Gurnett and Frank [1972].). Gurnett and Frank [1972] have hypothesized that the V-shape is due to the frequency dependence of the limiting ray angle for whistler mode propagation from the generation region down to the satellite. In other words the maximum angle with respect to $\vec{B}_o$ at which the wave may propagate increases as frequency increases, allowing high frequency waves to be observed further from the field line passing through the generation region.

To check the theory of Gurnett and Frank [1972] the V-shaped VLF hiss in their Plate 5 (reproduced here as Figure 12) was examined. The first V-shaped VLF hiss event at $22^h\ 55^m$ UT in Plate 5 has a width of about 1.6° in invariant latitude between points where the frequency of the outer edge of the V-shape is 5 kHz. The magnetic local time is changing very slowly at this point so that the

satellite is moving primarily in invariant latitude. The power program was used to calculate initial wave normal angles for Cerenkov generated waves for frequencies from 2—12 kHz at an altitude of 4000 km and an invariant latitude of 73°. The ray paths were then determined by the two-dimensional ray tracing program. The latitudes where the ray paths passed an altitude of 2500 km are shown in Figure 13. Although the shape of the expected spectrum from Figure 13 does not precisely match the shape of the event in Figure 12, their general appearance is similar. The width at 5 kHz is 1.45°, thus indicating that the generation altitude of this event would be slightly more than 4000 km if this model is correct. Gurnett and Frank [1972] estimated the altitude of the VLF hiss generation region to be about 5000—10,000 km. This is in reasonable agreement, especially since this example appears to be the narrowest of the V-shaped VLF hiss events in Figure 12.

The fact that there is less noise inside the outline of these events suggests that the characteristic size of the generation region is considerably less than the distance between the generation region and the satellite. An incoherent Cerenkov mechanism is probably not responsible for this VLF hiss since the precipitating electrons would radiate over much wider altitude range, producing a more incoherent spectrum. This decrease in power for higher frequencies is due to the increased angular dispersion of the ray. Even if the particles were confined to radiate in a source region of ~ 100 km,

the power radiated would not be sufficient to explain the observed power or electric field spectral density. The generation mechanism may be an instability or coherent Cerenkov radiation. The wave normal angle of the emission is probably near the resonance cone angle since the initial wave normal angles for Cerenkov emission were used in this calculation and are near the resonance cone.

If the satellite passed through the generation field line the observed minimum frequency of the emission would be the local f_{LHR} since these waves would travel with least deviation down the field line and reflect (reverse direction) at the satellite altitude. Higher frequency waves would be able to propagate below the satellite altitude, but lower frequency waves would reflect above the satellite. If the satellite were to pass to one side of the field line through the generation region the minimum observed frequency would not be the local f_{LHR}, but that frequency with a limiting ray angle large enough to propagate to the satellite. Such V-shaped VLF hiss events with variations in the lower cutoff frequency are observed. (See, for example, Figure 7 of Gurnett et al. [1971].)

V. SAUCERS

The last event at 22h 58m UT in Figure 12 was observed to be traveling up the field line. It is an example of a saucer-shaped emission, or a saucer. Observed with the Alouette 1 and 2 satellites (R. E. Barrington, personal communication, quoted by Mosier and Gurnett [1969]) and Injun 5 by Mosier and Gurnett [1969], Gurnett et al. [1971], and Gurnett and Frank [1972], saucers are often observed at low altitudes in the auroral zones. They range in frequency from less than 1 kHz to above 10 kHz and have a time duration from a few seconds to a few tens of seconds.

Mosier and Gurnett [1969] have presented a detailed theory explaining many of the characteristics of saucers. Its appearance on the spectrogram depends upon the same limiting ray-angle argument that was mentioned above for V-shaped VLF hiss. Basically, a source region below the satellite emits waves at frequencies above the f_{LHR} at the source which propagate upward. As the satellite passes over the source region, high frequency waves with large limiting ray angles are observed, followed by lower frequency waves with smaller limiting ray angles until the minimum frequency, the f_{LHR} at the source, is observed when the satellite passes through the field line connected to the source region. Then the frequency increases as the satellite moves away from the source field line and the limiting ray angle increases.

Figure 14 shows another example of a saucer observed with Injun 5. Mosier and Gurnett [1969] have made a detailed analysis of this saucer and from its width have deduced from limiting ray-angle considerations that the source was located at an altitude of 1400 km, about 1100 km below the satellite. Gurnett and Frank [1972] consider it likely that intense low-energy ($\sim$ 100 ev) streams of electrons are the particles which emit saucer radiation.

It is possible that the generation mechanism of saucers is incoherent Cerenkov radiation. To check this possibility and the theories of Mosier and Gurnett [1969] and Gurnett and Frank [1972], Cerenkov power and ray path calculations were performed to match the characteristics of the saucer observed at an altitude of 2500 km shown in Figure 14. Best agreement between the calculated and observed characteristics of the saucer in Figure 14, width ($\simeq$ 12 sec at 10 kHz) and lower-frequency cutoff ($\simeq$ 1.7 kHz), was found for a source altitude of 1800 km. Since no energetic electron spectrum has been measured in association with a saucer the electron spectrum measured by Westerlund [1969] was used in the Cerenkov power calculation (assumed to be flowing up the field lines, $\alpha > 90°$). The ray paths of the Cerenkov waves were then determined and the latitude of the waves at the altitude of 2500 km as a function of frequency is shown in Figure 15. The shape of the calculated saucer has no curvature as the observed saucers do. This curvature may be due to the small change of plasma parameters in the model over the 700 km ray path.

Assuming an emission region with a characteristic dimension of 100 km the spectral densities at 8 kHz were calculated to be

$$\frac{dP}{df} = 8 \times 10^{-17} \text{ w/m}^2\text{Hz}$$

$$\frac{dE^2}{df} = 5 \times 10^{-11} \text{ V}^2/\text{m}^2\text{Hz}$$

$$\frac{dB^2}{df} = 3 \times 10^{-33} \text{ Wb}^2/\text{m}^4\text{Hz} \quad .$$

The maximum wide band electric and magnetic fields measured during the saucer in Figure 14 were 5.6×10^{-3} volts and 1.9 mγ. Assuming a bandwidth of 2 kHz and an effective dipole antenna length of 2.85 m, the spectral densities can be calculated to be

$$\frac{dE^2}{df} = 1.9 \times 10^{-9} \text{ V}^2/\text{m}^2\text{Hz}$$

$$\frac{dB^2}{df} = 1.8 \times 10^{-27} \text{ Wb}^2/\text{m}^4\text{Hz} \quad .$$

The satellite electric antenna spectrum analyzer at 7.35 kHz measured a maximum voltage spectral density of 1.7×10^{-8} V^2/Hz giving an electric field spectral density of

$$\frac{dE^2}{df} = 2.1 \times 10^{-9} \ V^2/m^2Hz \quad ,$$

which agrees quite well with the measurement derived from the wide band electric field. Using the wide band measurements and assuming a cosine correlation of $\langle \cos \varphi \rangle = 0.5$ (see Gurnett and Frank [1972]) the lower limit of the power spectral density is calculated to be

$$\frac{dP}{df} = 7.4 \times 10^{-13} \ w/m^2Hz \quad .$$

The observed spectral densities are considerably higher than the ones calculated on the basis of incoherent Cerenkov radiation, i.e., a factor of 10^4 in power. Coherent Cerenkov radiation where groups of electrons radiate in phase might produce enough power to explain the intensity of saucers, or they may be produced by another collective action of radiating particles, for example an electrostatic or electromagnetic instability.

Since the envelope of saucers is usually sharply defined the emitting region must be a confined region rather than a line, sheet or extended source since any of these regions would tend to fill in the envelope of the saucer.

From the results obtained here, saucers appear most likely to be generated in a limited region below satellite altitudes at an altitude of a few thousand kilometers by the collective action of

low-energy upgoing electrons. The radiation apparently must be generated at wave normal angles near the resonance cone angle so that these ray angles will be large to enable the waves to diverge a few degrees in hundreds of kilometers of path length.

VI. FAST HISSLERS

Siren [1972] reported the observation from the ground VLF station at Byrd Station (invariant latitude = 71°) of bursts of auroral hiss. Showing evidence of whistler mode dispersion, they were of very short duration, a few tenths of a second or less at all frequencies. They were observed from 2 to 12 kHz with a maximum signal intensity of

$$\frac{dP}{df} = 1.1 \times 10^{-17} \text{ w/m}^2\text{Hz}$$

at 3 kHz. Whistler mode analysis of the fast hisslers by Siren [1972] indicated generation altitudes in the range of 10,000 to 22,000 km. Siren suggests that Cerenkov radiation at these altitudes may be responsible for fast hisslers.

Waves that are generated by the Cerenkov mechanism from electrons with energies less than a few tens of kev have wave normal angles that are very close to the resonance cone. As these waves propagate down the field lines their wave normal angles change, but remain within a few hundredths of a degree of the resonance cone angle. When waves near the resonance cone reach the altitude where their frequency is equal to the local f_{LHR} they reflect and begin going up the field line. So if fast hisslers are generated by the

Cerenkov mechanism the waves would need to somehow couple to waves with smaller wave normal angles to pass the altitude level where $f = f_{LHR}$. Hissler waves must also make the transition from the ionosphere where the index of refraction, n, is very large to the atmosphere where n is one. If the transition is thought of as a step in n, only waves with values of Δ, the angle between $\vec{k}$ and the radius vector, close to 180° will be able to refract into the atmosphere.

A calculation of Cerenkov power was performed for an altitude of 15,000 km, an invariant latitude of 71°, and a frequency of 3 kHz and the ray paths were calculated for the resulting waves. The power observed at a ground station may be calculated with the following formula:

$$\left(\frac{dP}{df}\right)_{gs} = \frac{dP}{dfdV} V \left[\frac{(\Delta \text{ lat})_{wave}}{(\Delta \text{ lat})_{emitters}}\right]^2 T_{MS}\, T_{IA}$$

where dP/dfdV is the volume emissivity, V is the emitting volume, $(\Delta \text{ lat})_{wave}$ is the spreading of the wave in latitude (longitude), $(\Delta \text{ lat})_{emitters}$ is the width of the particle precipitation region, T_{MS} is the transmission coefficient due to collisional attenuation along the ray path in the magnetosphere, and T_{IA} is the transmission coefficient of the wave resulting from the inefficient coupling from the ionosphere to the atmosphere. The energetic electron spectrum used was that measured by Ackerson and Frank [1972] during the auroral-VLF hiss-electron precipitation event described in section IV.

$(\Delta \text{ lat})_{wave}$ was determined with the ray path calculation to be 6.9° and $(\Delta \text{ lat})_{emitters}$ assumed to be 1.8° as before. The ray path transmission coefficient T_{MS} was found to be 0.9 (- 0.4 db). T_{IA} was estimated from maximum satellite and ground station VLF hiss observations of 1.5×10^{-11} w/m^{2}Hz [Mosier and Gurnett, 1972] and 10^{-14} w/m^{2}Hz [Helliwell, 1965] to be about 10^{-3}. Knowing the emissivity 1.07×10^{-21} w/m^{2}Hz and the observed spectral density 1.1×10^{-17} an estimate of 3000 km for the source region size results.

One of the fast hisslers presented by Siren [1972] had an indicated generation altitude of 15,000 ± 1300 km. So starting at an initial altitude of 15,000 km it was determined that there was a range of initial wave normal angles for which the waves would successfully reach ground level at $\lambda = 71°$. These ranges, as a function of frequency from 2—12 kHz, are shown in Figure 16. Therefore, if the generation point of this hissler was 15,000 km and the propagation of the waves to the ground involved no coupling to other wave normal angles, the initial wave normal angles of the waves had to be between 0.2° and 2.3° with respect to the magnetic field. To check to see if the model produced the same dispersion as the hissler, ray paths for frequencies from 2—12 kHz were calculated from an initial altitude of 15,000 to a final altitude of 100 km and dispersions compared to those scaled from the spectrogram of the hissler given in Siren [1972]. The comparison is shown in Figure 17 with the line drawn through the dispersion determined from the ray path calculations.

The small difference in the two dispersions indicates that the total electron content below 15,000 km was similar in the models used by Siren and in the ray path calculation.

From power considerations, fast hisslers may be generated by the Cerenkov mechanism, but if they are the initial waves must couple to waves with small wave normal angles to pass the point where $f = f_{LHR}$ and must have $\vec{k}$ vectors antiparallel to the radius vector in the ionosphere to reach the ground. If fast hisslers propagate to the ground directly their initial wave normal angles must be close to zero. No matter what the generation mechanism the generation must be limited to a few thousand kilometers in size and must turn on and off on the order of a tenth of a second since the ground observations show whistler mode dispersion.

VII. UHR NOISE

UHR noise is band-limited white noise that is commonly observed by rockets and satellites in the magnetosphere at frequencies for which max $(f_{ge}, f_{pe}) \leqslant f \leqslant f_{UHR}$, where $f_{UHR}^2 = f_{ge}^2 + f_{pe}^2$.

Reports of upper hybrid resonance (UHR) noise in the magnetosphere have been given by Walsh et al. [1964] using rocket data, Bauer and Stone [1968] using ATS III data, Harvey [1968] using Ariel II data, Gregory [1969] using Ariel III data, Barrington and Hartz [1969] using Alouette I and II data, Hartz [1969, 1970] and Barrington et al. [1971] using Alouette II data, Muldrew [1970] using ISIS I data, Shaw and Gurnett [private communication, 1973], and Mosier et al. [1973] using Imp-6 data.

Mosier et al. [1973] have reported observations of UHR noise from frequencies somewhat below f_{pe} to f_{UHR}. At the time of these 250 to 600 kHz observations Imp 6 was inside the plasmasphere. Shaw and Gurnett [private communication, 1973] have observed the electric field of UHR noise at 100 and 178 kHz inside the plasmasphere with another experiment on the Imp-6 spacecraft. Their experiment is calibrated to give electric and magnetic field spectral densities. They report typical electric field spectral densities of

$$\frac{dE^2}{df} = 10^{-14} \text{ to } 10^{-16} \text{ V}^2/\text{m}^2\text{Hz}$$

for 100 and 178 kHz noise in the plasmasphere at L values from 4.5 to 5 close to the equatorial plane, but the magnetic field of UHR noise is apparently too weak to be observed.

Alouette I and II have also observed UHR noise. The upper-frequency cutoff of the noise is generally at or near f_{UHR}, with the lower frequency-cutoff sometimes near max (f_{pe}, f_{ge}) and sometimes near min (f_{pe}, f_{ge}) for both $f_{pe} > f_{ge}$ and $f_{ge} > f_{pe}$. The noise is as large as 30—40 db above the background, but the noise level has not been reported in absolute terms. Barrington et al. [1971] show two samples of the noise intensity as a function of frequency from 0.2 to 7 MHz near the auroral zone in their Figure 1. Recording (a) was obtained near $\lambda = 73°$ with characteristic frequencies estimated by Barrington et al. to be $f_{pe} = 0.700$ MHz, $f_{ge} = 0.784$ MHz, and $f_{UHR} = 1.04$ MHz. Noise above background was observed from about 0.850 MHz to 1.07 MHz. Recording (b) was obtained near $\lambda = 66°$ where Barrington et al. estimated $f_{pe} = 0.182$ MHz, $f_{ge} = 0.517$ MHz, and $f_{UHR} = 0.545$ MHz. Noise limits were about 0.15 MHz and 0.638 MHz.

Cerenkov emission has been suggested as the mechanism responsible for UHR noise by Walsh [1964], Bauer and Stone [1968], Gregory [1969], Muldrew [1970], Laaspere et al. [1971], Lim and Laaspere [1972], and Mosier et al. [1973].

As with VLF hiss, large indices of refraction are required for the production of large powers in the UHR noise frequency range by low-energy electrons through the Cerenkov mechanism. Large

indices of refraction are required for the production of large powers in the UHR noise frequency range by low-energy electrons through the Cerenkov mechanism. Large indices of refraction exist for wave normal angles near the resonance cone angle for frequencies $\max (f_{pe}, f_{ge}) < f < f_{UHR}$. Typically there are four or more orders of magnitude difference in power production between frequencies in this range to those out of this range. The region of expected generation of Cerenkov noise from the ambient energetic electrons in the magnetosphere, that is, the region for which $\max (f_{pe}, f_{ge}) < f < f_{UHR}$ for a frequency of 178 kHz, is shown in Figure 18. This region corresponds to region 3 of the CMA diagram [Stix, 1962] bounded by $S = 0$ ($f = f_{UHR}$), $R =$ ($f = f_{ge}$), and $P = 0$ ($f = f_{pe}$).

Calculations in the model magnetosphere described above have been made at equatorial latitudes in the 100 and 178 kHz generation regions to see if the theoretical electric field spectral densities are near the ones observed by Imp 6. An energetic electron spectrum reported by Schield and Frank [1970] to be representative of the plasmasphere and assumed to be isotropic was used in the calculations. The spectrum is shown in Figure 3. For a single electron Cerenkov waves are generated with $\vec{k}$ vectors forming a cone around the earth's magnetic field with an opening angle of twice the wave normal angle. For a spectrum of electrons a representative wave normal angle is chosen, the one corresponding to that part of the spectrum with the largest power production. For an isotropic pitch angle distribution

of electrons there will be two representative cones, for electrons with pitch angles less than and greater than 90°.

The two-dimensional ray tracing program first determined the ray paths of those waves with $\vec{k}$ vectors in the meridian plane. The two rays which initially began decreasing in altitude went down until their wave frequencies f became very close to f_{pe}, at which point they turned around and began increasing in altitude until f became close to f_{UHR}. The attenuation of the waves after the first turn was from 2—4 db and 10—20 db ~ 200 km from the point where $f = f_{UHR}$. The two rays which initially began increasing in altitude continued until f became close to f_{UHR} where the attenuation again began increasing rapidly to over 10 db. Illustrative ray paths in two dimensions are shown in Figure 19 for a frequency of 178 kHz and a generation point on the equator at an altitude of 7100 km. The three-dimensional ray tracing program was then used to calculate ray paths for those initial $\vec{k}$ vectors out of the meridian plane. The ray paths for the upgoing rays were very similar to those in the meridian plane except that they moved in longitude as well as altitude and latitude. The initially downgoing nonmeridional rays, however, generally followed the same path but reversed directions, or reflected, at higher altitudes. They then continued upward until f approached f_{UHR} where attenuation again began increasing rapidly. These ray path calculations mean that at a point in the magnetosphere near the equatorial plane frequencies close to f_{UHR} should be strongest, decreasing toward f_{pe}.

The volume of space illuminating a one m^2 antenna in the UHR region is a one m^2 tube along the ray paths through that antenna since the region is fairly uniformly producing energy. To estimate power, electric and magnetic field spectral densities at a point in the UHR region, the contributions to the spectral density from points along the ray paths through the point are added, including the effects of attenuation along the path.

The fields were calculated at the observer's position from powers generated along the ray paths and added, giving the total field at the observation point due to all of the possible generation points. Approximate spectral densities at 178 kHz are found to be

$$\frac{dP}{df} = 10^{-15} \text{ w/m}^2\text{Hz} \quad ,$$

$$\frac{dE^2}{df} = 10^{-9} \text{ V}^2/\text{m}^2\text{Hz} \quad ,$$

$$\frac{dB^2}{df} = 10^{-32} \text{ Wb}^2/\text{m}^4\text{Hz} \quad ,$$

and at 100 kHz

$$\frac{dP}{df} = 10^{-15} \text{ w/m}^2\text{Hz} \quad ,$$

$$\frac{dE^2}{df} = 10^{-8}\ V^2/m^2Hz \quad ,$$

$$\frac{dB^2}{df} = 10^{-31}\ Wb^2/m^4Hz \quad .$$

The electric field spectral densities are considerably larger than those measured by Imp 6. But the magnetic field spectral densities are near the noise levels of the magnetic field spectrum analyzers on Imp 6 of

$$\left(\frac{dB^2}{df}\right)_{178\ kHz} = 2.6 \times 10^{-31}\ Wb^2/m^4Hz$$

and

$$\left(\frac{dB^2}{df}\right)_{100\ kHz} = 5.4 \times 10^{-32}\ Wb^2/m^4Hz$$

[R. Shaw, private communication, 1973].

There are at least three factors which may explain this apparent high electric field spectral density.

(1) The electron spectrum used may have been too intense which would reduce all three spectral densities.

(2) Due to thermal effects or wave normal scattering by irregularities some or all of the wave normal angles of the waves may have been

dispersed away from the resonance cone. Some initial wave normal angle dispersion will occur naturally from the range of $v_{\parallel}$ in the energetic electron spectrum. A change of one degree from the resonance cone angle will reduce the electric field spectral density by about two and one-half orders of magnitude and raise the magnetic field spectral density by the same factor.

(3) Thermal effects would also influence the power production. Trulsen [1971] notes that thermal effects dominate near the hybrid resonances. A finite temperature will reduce the maximum index of refraction, increasing the minimum particle velocity that can radiate. The resonance will also be spread in frequency, which may also explain the existence of power outside of the limits of the frequency range expected from cold plasma theory, max $(f_{pe}, f_{ge}) < f < f_{UHR}$. But account has not been taken of these thermal effects.

The electric field spectral density was calculated at points in the magnetosphere close to where the two recordings mentioned earlier [Barrington et al., 1971] were taken by Alouette II. The critical frequencies for the first calculation were f_{pe} = 0.688 MHz, f_{ge} = 0.817 MHz, and f_{UHR} = 1.07 MHz. The calculated electric field spectral density from 0.82 to 1.06 MHz is shown in Figure 20. The maximum spectral density of 5.8×10^{-8} V^2/m^2Hz is again considerably above the Imp-6 measurements. The only number that can be derived from Alouette reports is that an average maximum electric field is

44 db above the noise level at 200 kHz. Barrington et al. [1971] give a receiver bandwidth of 40 kHz and a noise level of 7.5×10^{-8} V/m. 44 db then corresponds to a spectral density of 2.5×10^{-15} V^2/m^2Hz. The spectrum shows no obvious similarity to recording (a).

For the second case the critical frequencies were $f_{pe} = 0.177$ MHz, $f_{ge} = 0.492$ MHz, and $f_{UHR} = 0.523$ MHz. Figure 21 shows the calculated electric field spectral density which is far in excess of the measured values. The three possible reasons given above for the difference between the calculated and observed spectral densities may be valid here too.

Cerenkov radiation from typical magnetospheric electron spectrums seems more than adequate to provide the power observed in UHR noise. The spectrums of calculated UHR noise are not obviously like those of observed UHR noise. Thermal effects on the generation and propagation of the waves may be responsible for the lower observed electric fields.

VIII. ELF HISS

ELF hiss, spectrograms of which are shown in Figure 22, is narrow-band (a few hundred to a few thousand Hz), white noise commonly observed with low-altitude satellites from 50° to 80° invariant latitude and 6 to 18 hours magnetic local time [Taylor and Gurnett, 1968]. Gurnett et al. [1971] found that ELF hiss was generally observed to be downgoing, but occasionally upgoing at invariant latitudes less than 60°. They found that the transition region between upgoing and downgoing ELF hiss was often the boundary between the plasmasphere and the light ion trough. They tentatively concluded that upgoing ELF hiss may be generated at high altitudes outside the plasmapause and reflected upwards at some point below the satellite after crossing the plasmapause boundary.

An intense ELF hiss event from Injun 5 has been analyzed to determine its approximate spectral densities. The orbital parameters at the time of largest intensity were: altitude = 2174 km, invariant latitude = 47.6°, magnetic local time = 15.6 hours. The measured wide band field intensities were E = 50 mV and B = 6.5 mγ. The bandwidth was estimated to be 300 Hz and a cosine correlation of 0.5 was assumed. Spectral densities of

$$\frac{dE^2}{df} = 1.0 \times 10^{-6} \ V^2/m^2Hz \quad ,$$

$$\frac{dB^2}{df} = 1.4 \times 10^{-25} \text{ Wb}^2/\text{m}^4\text{Hz} \quad ,$$

$$\frac{dP}{df} = 1.5 \times 10^{-10} \text{ w/m}^2\text{Hz}$$

were calculated. These spectral densities appear to be the strongest spectral densities to have been reported for VLF emission. ELF hiss was found to be the strongest VLF emission observed with Injun 3 also [Taylor and Gurnett, 1968].

The white noise character of ELF hiss suggests that Cerenkov emission may be its generation mechanism. However, the facts that Cerenkov power is generated near the resonance cone and that down-going waves with such wave normal angles reflect when their wave frequency approaches f_{LHR} seem to rule out the Cerenkov mechanism. The lower-frequency cutoff of ELF hiss was determined by Gurnett and Burns [1968] to be usually below the proton gyrofrequency, f_{gH^+}, which is a considerably lower frequency than f_{LHR}. The observed power spectral density of ELF hiss is also two and one-half orders of magnitude above the largest power expected from perfectly guided incoherent Cerenkov radiation from an auroral zone flux tube from the results shown in Figure 4. In addition, Figure 8 shows that the largest contribution of 1 kHz power is from equatorial regions. Even if the power were generated at angles other than those near the resonance cone, ray path calculations show that 800 Hz waves will not

propagate to satellite altitudes from initial altitudes greater than 19,000 km starting on the 65° invariant latitude field lines. At 15,000 km initial wave normal angles from - 10° $\leq \psi_o \leq$ 0° will propagate to satellite altitudes and this range widens as the initial altitude decreases, to - 60° $\leq \psi_o \leq$ 40° at an initial altitude of 5000 km.

It was thought that ray path calculations of waves with ELF hiss frequencies would be able to confirm the theory of Gurnett et al. [1971] predicting the reflection of downgoing ELF hiss at low altitudes near the plasmapause. They predict that ELF hiss waves would travel to significantly lower latitudes while reflecting at low altitudes, resulting in the occasionally observed change from downgoing outside the plasmapause to upgoing within the plasmapause. The two-dimensional ray tracing program was used to calculate ray paths for initial altitudes above satellite altitudes and for invariant latitudes slightly larger than 60° (the invariant latitude of the L = 4 plasmapause). The rays did reflect at the L = 0 cutoff as predicted by Gurnett and Burns [1968] but the decrease in latitude was never more than a few degrees. Gurnett et al. [1971] show an example of ELF hiss which changes direction (their Figure 5) at an invariant latitude of about 59°. Inspection of the original data shows that the ELF hiss was upgoing at invariant latitudes from 38° to 59° and downgoing from 59° to 69°. The satellite altitude and magnetic local time stayed nearly constant during the ELF hiss event

at about 2400 km and 6^h, respectively. For the ELF hiss waves to be observed downgoing and then upgoing at least some waves in this event would have had to propagate 20° in invariant latitude (~ 1000 km) at altitudes below 2400 km. The magnetosphere model used here will not reproduce such behavior, but perhaps occasionally there are horizontal ducts to produce large latitudinal displacements of ELF hiss propagation paths.

An alternative explanation of the behavior may be that the generation region is below satellite altitudes in the plasmasphere and that the waves propage upwards and then reflect at high altitudes, coming down outside the plasmasphere at higher latitudes. Two objections to this theory are immediate, however. First, the generation region would necessarily be small implying a very large volume emissivity in a region without large electron fluxes. Second, there appear to be no plasma cutoffs or resonances capable of reflecting upgoing waves above satellite at ELF frequencies. Ray path calculations confirmed that there are no reflections of upgoing ELF hiss frequency waves starting in the plasmasphere above satellite altitudes.

On the basis of the observations and the calculations presented here, it seems most likely that the generation mechanism for ELF hiss is a particle cooperative one, for example coherent Cerenkov radiation or a wave-particle instability. The generation region appears to be at altitudes above a few thousand kilometers but below

a few tens of thousands of kilometers near the plasmapause or at slightly higher latitudes. The waves propagate down the field lines and reflect at the L = 0 cutoff, sometimes propagating to lower latitudes at low altitudes.

IX. DISCUSSION

A. Applicability of the Theory

There are two assumptions in the Cerenkov theory which should be closely examined, the assuptions that the plasma is cold and that the test particles and the radiation they emit have no effect on the plasma. Trulsen [1971] states that thermal effects are particularly important in a plasma near the hybrid resonances where $\epsilon_1 = 0$ in cold plasma theory, implying that thermal effects are important in the consideration of VLF hiss and UHR noise. A finite temperature may be introduced into the theory by using the Vlasov equation to determine the dielectric tensor describing the plasma [Trulsen, 1971] or by introducing a temperature dependent pressure term in the equation of motion. In either development ϵ_1 does not go to zero at the hybrid resonances. Because of this fact Trulsen [1971] claims that the Cerenkov power spectra is changed 'completely' from the cold plasma result near f_{UHR}, removing the singularity in the spectra at $f = f_{UHR}$ and extending the spectrum far above f_{UHR}. A finite temperature will, in smearing out the resonance, reduce the maximum index of refraction n. This reduction in the maximum n will reduce the power emitted from an electron spectrum by increasing the minimum parallel particle velocity that will radiate.

Some theoretical calculations may be made to determine the necessity of including thermal effects in the power and ray tracing

theories. For cold plasma theory to be valid β (gas energy density/ magnetic energy density) should be much less than one. In an extreme case magnetospheric plasma parameters might be $B_o = 0.4$ G, $n = 10^6$ cm^{-3}, and $T = 10^5$ °K, which gives a β of 2×10^{-3}. The component of the phase velocity of the emitted wave along $\vec{B}_o$, $v_{ph,\parallel}$, should be considerably higher than the mean electron thermal velocity. With the choice of collisions as a dissipative force and the numbers used in the calculation, the thermal velocity was as large as $v_{ph,\parallel}$. Perhaps some of the discrepancies that do exist between theory and observation presented here are explicable in terms of thermal effects. Because of the much more complicated dispersion relation it was necessary to assume zero temperature in order to obtain a reasonable numerical description of the plasma, however.

The assumption that the particles and the emitted waves have no effect on the plasma may also be considered. It will be shown later in this section that the conversion efficiency from particle energy to VLF hiss wave energy is no larger than about 10^{-7}. Therefore the wave energy is much less than the particle energy, so that neither the wave emission nor the propagating waves can affect the particle spectrum. In the case of VLF hiss it may be that the emitted waves do interact with the plasma and energetic particles, causing coherent emission which greatly increases the wave energy output. (This possibility will be briefly considered later.)

B. Validity of the Programs

The program which calculates the power emitted by a particle has been checked against published data of similar calculations by Jørgensen [1967] and Lim and Laaspere [1972]. In these checks the collision frequency was taken to be zero to agree with the previously reported calculations. Jørgensen's Figure 10 was the basis of the first comparison. With the plasma parameters given for an altitude of 10^4 km, the power was calculated for five frequencies and was within about 5% of the value read from the figure.

Figure 1 of Lim and Laaspere [1972] provided the second comparison for the power program. Again using the plasma parameters listed, at a frequency of $1/2\ f_{ge}$ the power was calculated for four energies. The calculations and the data from Lim and Laaspere's figure agree to within about 5%.

Three tests were made of the ray tracing program to insure its validity. The first test was for a ray path in a horizontally stratified medium. The plasma density and magnetic field were assumed to vary only in the vertical direction, implying that the index of refraction varies only vertically. A coordinate transformation from rectangular to polar coordinates was used to make full use of the original expressions in the program. In this medium k_h, the component of $\vec{k}$ in the horizontal direction should be constant (Snell's law). In a test where only the plasma density varied k_h was constant to within 0.04% until the wave normal angle was 0.04

degrees from the resonance cone angle. At this point roundoff errors are expected to be large. Varying both the magnetic field and the plasma density resulted in k_h constant to within 0.008% for frequencies more than 0.04% away from f_{ge}, where roundoff errors are also expected to be large.

It was shown by Shawhan [1966] that if a ray is reversed it must retrace the same ray path. This characteristic of ray paths provides a means of checking the integration accuracy of the program. This reversibility check was made, and for a two-way distance of 16,000 km, the ray returned to within 0.001% of its starting point, compared to the one-way distance of 8000 km and to within 0.001% of its initial wave normal angle.

Finally, the ray tracing programs were compared to that of Kimura [1966] by reproducing the ray path he calculated in his Figure 6. The plasma density model involved was an electron-three-ion diffusive equilibrium model and the magnetic field was represented by a centered dipole. For a frequency of 1 kHz, an initial altitude of 300 km, an initial latitude of 30°, and an initial wave normal angle (with respect to the radius vector) of 0°, ray paths were calculated. The turning points (latitude maximums) found by Kimura were given in his Table 4. The turning points found here agree to within a few percent in altitude and latitude of the ones found by Kimura.

C. Coherent and Amplified Cerenkov Radiation

The Cerenkov power calculation presented here for several magnetospheric wave phenomena, as in Jørgensen [1968] and Lim and Laaspere [1972] for VLF hiss, assumed that each electron radiated independently, that is, with random phase. The total power P_T radiated incoherently by n particles is

$$P_T = nP$$

where P is the power radiated by each particle. On the other hand, if the n particles radiated coherently, that is, all with the same phase, the total power would be

$$P_T = n^2 P \quad .$$

Therefore, if the electrons are radiating somewhat coherently in the Cerenkov mode an approximately square law relation between electron and VLF fluxes would be expected since the radiating power is proportional to the square of the number of radiating electrons. It is clear that a relatively small number of electrons emitting Cerenkov radiation coherently could substantially increase the power to the observed levels.

The threshold effect in the relationship between low-energy (~ 100 ev) electrons and VLF hiss found by Gurnett and Frank [1972]

for VLF hiss might be due to the steepness of the square law being mistaken for a threshold or it may be that there is a threshold corresponding to the onset of an instability at 10^4—10^5 elec/cm^2 sec ev ster. The observation by Gurnett and Frank [1972] showed VLF hiss power changing about 3 1/2 orders of magnitude while the particle flux changed by about 1 1/2 orders of magnitude which is approximately square law, which suggests partially coherent Cerenkov radiation.

Singh [1972] has found that Cerenkov waves may be amplified by a factor up to three orders of magnitude by interaction with an electron beam. Significant amplification factors for an interaction length of 1000 km were found in the frequency range $0.1\ f_b \leq f \leq f_b$, where f_b is the plasma frequency of the beam. For a beam density of 1 cm^{-3} (typical for the spectra in Figure 3), Cerenkov waves would be amplified in the frequency range $0.9 \leq f \leq 9$ kHz. Singh's calculations, however, assumed a longitudinal dispersion relation. If similar results are valid for wave normal angles near the resonance cone angle, VLF hiss may be explicable in terms of amplified Cerenkov radiation.

D. Instabilities

There are a number of plasma instability mechanisms that have been proposed to explain various magnetospheric wave phenomena.

Kennel and Petschek [1966] have determined that the whistler mode is unstable to wave growth when the energetic electron pitch angle distribution is sufficiently anisotropic, favoring perpendicular

velocities. The whistler mode noise is generated at high altitudes near the equatorial plane at the electron gyrofrequency and may be Doppler shifted into the VLF frequency range.

The generation mechanism for VLF and ELF hiss and other phenomena may involve generation of waves in the drift mode at frequencies between the ion and electron gyrofrequencies and subsequent coupling to the whistler mode [Sizonenko and Stepanov, 1967]. The fastest growing whistler mode has a frequency given by

$$f = \frac{u_\perp}{2v_i} \sqrt{f_{ge}\, f_{gi}}$$

where $u_\perp$ is the ion velocity perpendicular to $\vec{B}_o$ due to the influence of an ion cyclotron wave and v_i is the ion thermal velocity. In the high plasma frequency limit $(f_{ge}\, f_{gi})^{1/2}$ is the lower hybrid resonance frequency (f_{LHR}) (which is usually assumed to be the lower-frequency cutoff of VLF hiss). Therefore this fastest-growing whistler mode is in the correct frequency range for VLF phenomena.

Lee, Kennel, and Kindel [1971] found a high-frequency (near f_{LHR}) Hall current instability due to electron and ion drifts perpendicular to $\vec{B}_o$. They determined that this instability could produce waves in the ELF and part of the VLF frequency band.

Further consideration of these generation mechanisms is not undertaken here, but it seems clear that many of the wave phenomena

must be due to cooperative plasma effects, perhaps one or more of the instabilities mentioned above.

X. JUPITER

Jupiter is known to emit intense bursts of decametric radiation up to 10^{-19} w/m^{2}Hz for frequencies less than 40 MHz [Carr and Gulkis, 1969 and Warwick, 1967]. Some of this radiation is associated with the orbital position of the satellite Io and is made up of microsecond bursts which drift in frequency. This frequency and time structure might be attributed to particles passing through a region with varying plasma parameters and emitting radiation characteristic of the plasma [Warwick, 1963].

Assuming that the characteristic frequency is the electron gyrofrequency, incoherent Cerenkov (s = 0) and cyclotron (s = 1, 2) power calculations were made at 26 MHz. A model Jovian magnetosphere with a centered dipole magnetic field was assumed to give a maximum gyrofrequency at the latitude of Io's field line at the Jovian surface of about 40 MHz and the magnetosphere was assumed to be a hydrogen plasma in diffusive equilibrium. An estimate of the energetic electron spectrum emitted and accelerated by Io [R. Hubbard, 1972] up to 300 keV was used in the power calculation. Estimating the r^{-2} power loss from the initial spread in ray angles the received power at the surface of the earth was calculated to be about 10^{-33} w/m^{2}Hz. This is a factor of about 10^{14} less than observed during decametric bursts. The power from the s = 0 and 1 modes were nearly

equal and the power from the s = 2 mode was a factor of two lower than the power from the s = 1 mode. The observed rapid time variations and this power deficit calculated for incoherent radiation suggest that the emission mechanism is a coherent one. The coherence in time or space might be expected to be short, which would give a bursty character to the emitted radiation.

XI. CONCLUSIONS

The calculations of the power of incoherent Cerenkov radiation and the ray paths of resulting waves have been helpful in understanding the characteristics of some broadband LF, VLF, and ELF observations near the earth. Qualitative and quantitative comparisons between the theory and observations of VLF hiss, saucers, fast hisslers, UHR noise, and ELF hiss have been made. Calculation of decametric radiation from Jupiter have also been made. The results of these calculations are summarized below:

(1) VLF hiss. A calculation of expected VLF hiss power using an electron spectrum measured by Injun 5 was compared to a simultaneous observation of VLF hiss on the same spacecraft. The calculation included collisions and an estimate of thermal effects. Ray path calculations from the presumed generation region above the satellite were used to determine theoretical spectral densities and shapes. The power and magnetic field calculated were below observed levels by factors of $10^{2.5}$ and 10^{5}, but the electric field calculated a factor of three above observed levels.

From Injun 5 data, VLF hiss waves were determined to be propagating at wave normal angles about six degrees from the resonance cone. When the spectral densities of the fields were calculated for such a wave normal angle they were each about two orders of magnitude below the observed spectral densities. The

calculated spectral shape of VLF hiss agreed well with observed spectra, however. This agreement was due to larger latitudinal and longitudinal spreading of the higher frequency waves from a source region confined to the flux tube of the electron precipitation region. Nevertheless, it seems unlikely that VLF hiss is generated by incoherent Cerenkov radiation from electrons.

The calculated spectral shape of V-shaped VLF hiss is similar to observations when a source region limited in altitude extent at approximately 4000 km altitude was assumed. However, because of the small emitting volume the output power was low, which reduces the likelihood that the observed power is generated by completely incoherent Cerenkov radiation.

(2) Saucers. Ray path calculations defining the spectral shape of saucers tend to confirm the theory that the generation region is below the satellite and that the emission is caused by upcoming electrons. The characteristic size of the source region must be only a few hundred kilometers since the envelope of the saucer is well defined. The generation mechanism appears not to be incoherent Cerenkov due to the low power available from the small source region. The initial wave normal angle for the emission mechanism appear to be very close to the resonance cone angle.

(3) Fast hisslers. Ray path calculations show that the generation regions of fast hisslers are at high altitudes, e.g. 15,000 km. Incoherent Cerenkov radiation produces enough power with a generation region size of a few thousand kilometers to match the

observations of fast hisslers, but the short emission time and the apparent inability of Cerenkov waves (with initial wave normal angles near the resonance cone) to reach the ground from these altitudes argue against the Cerenkov mechanism. Only a small range of initial wave normal angles nearly aligned with the magnetic field (0.2°—2.3°) initially will reach the ground from an altitude of 15,000 km. It might be that this Cerenkov noise is momentarily scattered into a downgoing wave normal range, but this irregular scattering structure has not been considered.

(4) UHR noise. Observations of UHR noise show wider spectral shapes and lower spectral densities than calculated from incoherent Cerenkov radiation. Thermal effects may reduce the spectral density and change the spectral shape by increasing the minimum energy which an electron must have to Cerenkov radiate and by altering the wave normal angle distribution. Thermal effects would broaden the resonance, reducing the maximum possible index of refraction and increasing the range of emitted wave normal angles. This change in the dispersion relation would effect propagation as well as generation. Since the calculated power was above the observed power, it is possible that a calculation including thermal effects would predict well the characteristics of UHR noise.

(5) ELF hiss. Observed power levels and wide ranges of occurrence in latitude and longitude for ELF hiss are not consistent with

calculations of incoherent Cerenkov radiation. In addition, for these frequencies wave normal angles near the direction of the magnetic field are required for wave propagation from high altitudes to satellite altitudes.

(6) Jupiter. Incoherent Cerenkov (s = 0) and cyclotron (s = 1, 2) radiation from electrons emitted from Io and accelerated by Io's sheath electric field was found to be fourteen orders of magnitude less than observed during decametric bursts. Most of the power was calculated to be propagating perpendicular to Jupiter's magnetic field.

Table 1

Observed and Calculated VLF Hiss Intensities

Observation	Frequency kHz	Reference	dE^2/df V^2/m^2Hz	dB^2/df Wb^2/m^4Hz	dP/df w/m^2Hz
Alouette 2	10.	Barrington et al. [1971]	3×10^{-11}		(2×10^{-13})
Ground Station	5.	Helliwell [1965]			10^{-14}
Injun 3	8.8	Gurnett [1966]		4×10^{-28}	(10^{-12})
Injun 5	1-2	Mosier and Gurnett [1972]	1.4×10^{-8}	9.6×10^{-26}	1.5×10^{-11}
OGO 2	18.5	Jørgensen [1968]		10^{-25}	
OGO 6	audio	Laaspere et al. [1971]	10^{-9}		(6×10^{-12})
Cerenkov Calculations					
Jørgensen [1968] (peak intensity at 10 kHz)					10^{-14}
Lim and Laaspere [1972] (peak intensity at 70 kHz)					1.2×10^{-13}
Present results, basic calculation (peak intensity at 10 kHz)					3.5×10^{-13}
Improved calculation (peak intensity at $f_{LHR} = 1.45$ kHz)			5×10^{-8}	1×10^{-30}	5×10^{-14}
Calculation including wave normal angle dispersion			1×10^{-8}	7×10^{-28}	5×10^{-14}
Calculation for wave normal angle distribution peaked near 6° from the resonance cone			4×10^{-11}	1×10^{-27}	5×10^{-14}

( ) indicates powers calculated from a single field

Page Intentionally Left Blank

Page Intentionally Left Blank

LIST OF REFERENCES

Ackerson, K. L., and L. A. Frank, Correlated satellite measurements of low-energy electron precipitation and ground-based observations of an auroral arc, J. Geophys. Res., 77, 1128, 1972.

Barrington, R. E., and T. R. Hartz, Resonances observed by the Alouette topside sounders, in Plasma Waves in Space and Laboratory, edited by J. O. Thomas and B. J. Landmark, University Press, Edinburgh, 1969.

Barrington, R. E., T. R. Hartz, and R. W. Harvey, Diurnal distribution of ELF, VLF, and LF noise at high latitudes as observed by Alouette 2, J. Geophys. Res., 76, 5278, 1971.

Bauer, S. J., and R. G. Stone, Satellite observations of radio noise in the magnetosphere, Nature, 218, 1145, 1968.

Carr, T. D., and S. Gulkis, The magnetosphere of Jupiter, Rev. Astro. and Astrophys., 7, 577, 1969.

Dowden, R. L., Geomagnetic noise at 230 kc/s, Nature, 187, 677, 1960.

Dowden, R. L., Theory of generation of exospheric very-low-frequency noise (hiss), J. Geophys. Res., 67, 2223, 1962.

Eidman, V. Ia., The radiation from an electron moving in a magnetoactive plasma, J. Exptl. Theoret. Phys. (USSR), 34, 131, 1958; English translation, Sov. Phys.—JETP, 7, 91, 1958.

Eidman, V. Ia., Correction to the paper by V. Ia. Eidman, "The radiation from an electron moving in a magnetoactive plasma," J. Expltl. Theoret. Phys. (USSR), 36, 1335, 1959; English translation, Sov. Phys.—JETP, 9, 947, 1959.

Ellis, G. R. A., Low-frequency radio emission from aurorae, J. Atmos. and Terr. Phys., 10, 302, 1957.

Ellis, G. R. A., Low-frequency electromagnetic radiation associated with magnetic disturbances, Planet. Space Sci., 1, 253, 1959.

Ellis, G. R. A., Directional observations of 5 kc/s radiation from the earth's outer atmosphere, J. Geophys. Res., 65, 839, 1960.

Evans, D. S., Rocket observations of low energy auroral electrons, NASA Rept. X-611-66-376, NASA/GSFC, Greenbelt, Maryland, 1966.

Gallet, R. M., and R. A. Helliwell, Origin of very low frequency emissions, J. Res. Natl. Bur. Std. (U.S.), 63D, 21, 1959.

Gershman, B. N., and U. Yu. Trakhtengerts, Very-low-frequency radio emission of the upper atmosphere and its relationship with other geophysical phenomena, Usp. Fiz. Nauk, 89, 201, 1966; English translation, Sov. Phys.—Usp., 9, 414, 1966.

Gintsburg, M. A., Electromagnetic radiation of solar corpuscular streams, Phys. Rev. Letters, 7, 399, 1961.

Gregory, P. C., Radio emission from auroral electrons, Nature, 221, 350, 1969.

Gurnett, D. A., A satellite study of VLF hiss, J. Geophys. Res., 71, 5599, 1966.

Gurnett, D. A., and T. B. Burns, The low-frequency cutoff of ELF emissions, J. Geophys. Res., 73, 7437, 1968.

Gurnett, D. A., S. R. Mosier, and R. R. Anderson, Color spectrograms of very-low-frequency Poynting flux data, J. Geophys. Res., 76, 3022, 1971.

Gurnett, D. A., and L. A. Frank, VLF hiss and related plasma observations in the polar magnetosphere, J. Geophys. Res., 77, 172, 1972.

Hartz, T. R., Radio noise levels within and above the ionosphere, Proc. IEEE, 57, 1042, 1969.

Hartz, T. R., Low-frequency noise emissions and their significance for energetic particle processes in the polar ionosphere, in The Polar Ionosphere and Magnetospheric Processes, edited by G. Shovli, Gordon and Breach, New York, 1970.

Harvey, C. C., Radio emission from geomagnetically trapped particles, Nature, 217, 50, 1968.

Helliwell, R. A., Whistlers and Related Ionospheric Phenomena, Stanford University Press, Stanford, California, 1965.

Hubbard, R. F., A sheath model for the acceleration of charged particles from Jupiter's moon Io, M. S. Thesis, University of Iowa, Iowa City, Iowa, 1972.

James, H. G., Whistler-mode hiss at low and medium frequencies in the dayside-cusp ionosphere, submitted to J. Geophys. Res., 1973.

Jørgensen, T. S., Interpretation of auroral hiss measured on OGO 2 and at Byrd station in terms of incoherent Cerenkov radiation, J. Geophys. Res., 73, 1055, 1968.

Kennel, C. F., and H. E. Petschek, Limit on stably trapped particle fluxes, J. Geophys. Res., 71, 1, 1966.

Kimura, I., Effects of ions on whistler-mode ray tracing, Radio Science, 1, 269, 1966.

Kindel, J. M., and C. F. Kennel, Topside current instabilities, J. Geophys. Res., 76, 3055, 1971.

Laaspere, T., W. C. Johnson, and L. C. Semprebon, Observations of auroral hiss, LHR noise, and other phenomena in the frequency range 20 Hz to 540 kHz on OGO 6, J. Geophys. Res., 76, 4477, 1971.

Lee, K., C. F. Kennel, and J. M. Kindel, High-frequency Hall current instability, Radio Science, 6, 209, 1971.

Liemohn, H. B., Radiation from electrons in magnetoplasma, Radio Science, 69D, 741, 1965.

Lim, T. L., and T. Laaspere, An evaluation of Cerenkov radiation from auroral electrons with energies down to 100 ev, J. Geophys. Res., 77, 4145, 1972.

MacArthur, J. W., Theory of the very low frequency radio emissions from the earth's exosphere, Phys. Rev. Letters, 2, 491, 1959.

Mansfield, V. N., Radiation from a charged particle spiraling in a cold magnetoplasma, Astrophys. J., 147, 672, 1967.

McEwen, D. J., and R. E. Barrington, Some characteristics of the lower hybrid resonance noise bands observed by the Alouette 1 satellite, Can. J. Phys., 45, 13, 1967.

McKenzie, J. F., Cerenkov radiation in a magneto-ionic medium (with application to the generation of low-frequency electromagnetic radiation in the exosphere by the passage of charged corpuscular streams), Phil. Trans. Roy. Soc. London, A255, 585, 1963.

McKenzie, J. F., Radiation losses from a test particle in a plasma, Phys. Fluids, 10, 2680, 1967.

Melrose, D. B., The absorption of waves by charged particles in magnetized plasmas, Astrophys. and Space Sci., 2, 171, 1968.

Mosier, S. R., and D. A. Gurnett, VLF measurements of the Poynting flux along the geomagnetic field with the Injun 5 satellite, J. Geophys. Res., 74, 5675, 1969.

Mosier, S. R., and D. A. Gurnett, Observed correlations between auroral and VLF emissions, J. Geophys. Res., 77, 1137, 1972.

Mosier, S. R., M. L. Kaiser, and L. W. Brown, Observations of noise bands associated with the upper hybrid resonance by the Imp-6 radio astronomy experiment, J. Geophys. Res., 78, 1673, 1973.

Muldrew, D. B., Preliminary results of ISIS I concerning electron-density variations, ionospheric resonances, and Cerenkov radiation, Space Res., 10, 786, 1970.

Murcray, W. B., and J. H. Pope, Doppler-shifted cyclotron frequency radiation from protons in the exosphere, Phys. Rev. Letters, 4, 5, 1960.

Murcray, W. B., and J. H. Pope, Energy Fluxes from the cyclotron radiation model of VLF radio emission, Proc. IRE, 49, 811, 1961.

Nicolet, M., The collision frequency of electrons in the ionosphere, J. Atmos. and Terr. Phys., 3, 200, 1953.

Sachs, D. L., Effect of collisions on ion cyclotron waves, Phys. Fluids, 8, 1520, 1965.

Santirocco, R. A., Energy fluxes from the cyclotron radiation model of VLF radio emission, Proc. IRE, 48, 1650, 1960.

Schield, M. A., and L. A. Frank, Electron observations between the inner edge of the plasma sheet and the plasmasphere, J. Geophys. Res., 75, 5401, 1970.

Seshadri, S. R., and H. S. Tuan, Radiation from a uniformly moving charge in an anisotropic, two component plasma, Radio Science, 69D, 767, 1965.

Shawhan, S. D., VLF ray tracing in a model ionosphere, U. of Iowa Res. Rept. 66-33, 1966.

Shawhan, S. D., Behavior of VLF ray paths in the ionosphere, U. of Iowa Res. Rept. 67-25, 1967.

Singh, R. P., Amplification of signal by Cerenkov resonance interaction, Planet. Space Sci., 20, 2073, 1972.

Siren, J. C., Dispersive auroral hiss, Nature, 238, 118, 1972.

Sizonenko, V. L., and K. N. Stepanov, Plasma instability in the electric field of an ion-cyclotron wave, Nucl. Fus., 7, 131, 1967.

Spitzer, L., The Physics of Fully Ionized Gases, Interscience, New York, 1956.

Stix, T. H., The Theory of Plasma Waves, McGraw-Hill, New York, 1962.

Taylor, W. W. L., and D. A. Gurnett, Morphology of VLF emissions observed with the Injun 3 satellite, J. Geophys. Res., 73, 5615, 1968.

Trulsen, J., Cyclotron radiation in hot magnetoplasmas, J. Plasma Phys., 6, 367, 1971.

Trulsen, J., and J. A. Fejer, Radiation from a charged particle in a magnetoplasma, J. Plasma Phys., 4, 825, 1970.

Walsh, D., F. T. Haddock, and H. F. Schulte, Cosmic radio intensities at 1.225 and 2.0 Mc measured up to an altitude of 1700 km, Space Res., 4, 935, 1964.

Warwick, J. W., Dynamic spectra of Jupiter's decametric emission, 1961, Astrophys. J., 137, 41, 1963.

Warwick, J. W., The radiophysics of Jupiter, Space Sci. Rev., 6, 841, 1967.

Westerlund, L. H., The auroral electron energy spectrum extended to 45 ev, J. Geophys. Res., 74, 351, 1969.

FIGURE CAPTIONS

Figure 1 Three representations of an index of refraction surface for $f_{LHR} < f < 1/2\ f_{pe}$.

Figure 2 A spectrogram showing VLF hiss when the satellite was near an auroral arc [after Mosier and Gurnett, 1972].

Figure 3 Energetic electron energy spectra used in previous and present calculations of magnetospheric noise generated by the Cerenkov mechanism.

Figure 4 The spectral density of observed VLF hiss and of calculated incoherent Cerenkov radiation by various investigators.

Figure 5 The variation of wave normal angles over a ray path as a function of altitude for downward propagating VLF hiss waves. The wave normal angles stay very close to the resonance cone angle over the entire path.

Figure 6 The latitude dispersion of VLF hiss ray paths for frequencies of 2 and 10 kHz and two generation altitudes on the 70° invariant latitude field line.

Figure 7 The electron density derived from an electron-three ion diffusive equilibrium model of the magnetosphere with a plasmapause at L = 4.

Figure 8 The incoherent Cerenkov power emitted in altitude segments up to 48,000 km altitude at 70° invariant latitude.

Figure 9 Power and electric and magnetic field spectral densities expected from Cerenkov radiation from auroral electrons at an altitude of 2500 km.

Figure 10 The dependence of electric and magnetic field spectral densities upon wave normal angle for a typical VLF hiss wave at 2500 km.

Figure 11 The emission intensity for an auroral electron spectrum for various modes. The $s = 0$ (the Cerenkov mode) dominates from f_{LHR} to frequencies slightly below f_{pe}. The $s > 0$ modes are called normal cyclotron modes and the $s < 0$ modes are called anamolous cyclotron modes.

Figure 12 The spectrogram depicting downgoing V-shaped VLF hiss from 22h 54m 50s to 22h 57m 50s and an upgoing saucer centered at 22h 58m 00s after Gurnett and Frank [1972] (originally in color in their Plate 5).

Figure 13 The latitudes at which theoretical V-shaped VLF hiss waves pass an altitude of 2500 km for a generation region at an altitude of 4000 km and invariant latitude of 73°.

Figure 14 A spectrogram showing an intense upgoing saucer after Gurnett et al. [1971] (originally in color in their Figure 6).

Figure 15 The latitudes at which theoretical saucer waves pass an altitude of 2500 km for a generation region at an altitude of 1800 km and an invariant latitude of 69.5°.

Figure 16 The range of initial wave normal angles that will propagate into the earth-ionosphere waveguide for a generation altitude appropriate for fast hisslers (15,000 km) at an invariant latitude of 71° (Byrd Station).

Figure 17 Theoretical and experimental fast hissler dispersions from 2—12 kHz.

Figure 18 The 178 kHz cold plasma UHR noise generation region.

Figure 19 178 kHz UHR noise ray paths from a isotropic electron spectrum at an altitude of 7100 km on the geomagnetic equator. Note the reflections at f_{pe} and the attenuation of the waves.

Figure 20 A theoretical UHR noise electric field spectrum near 1 MHz in the auroral zone.

Figure 21 A theoretical UHR noise electric field spectrum near 0.5 MHz in the auroral zone.

Figure 22 A spectrogram of ELF hiss observed with the Injun 3 satellite.

INDEX OF REFRACTION SURFACE FOR F = 8 KHz, ALTITUDE = 2500 KM, F_{LHR} = 5.99 KHz

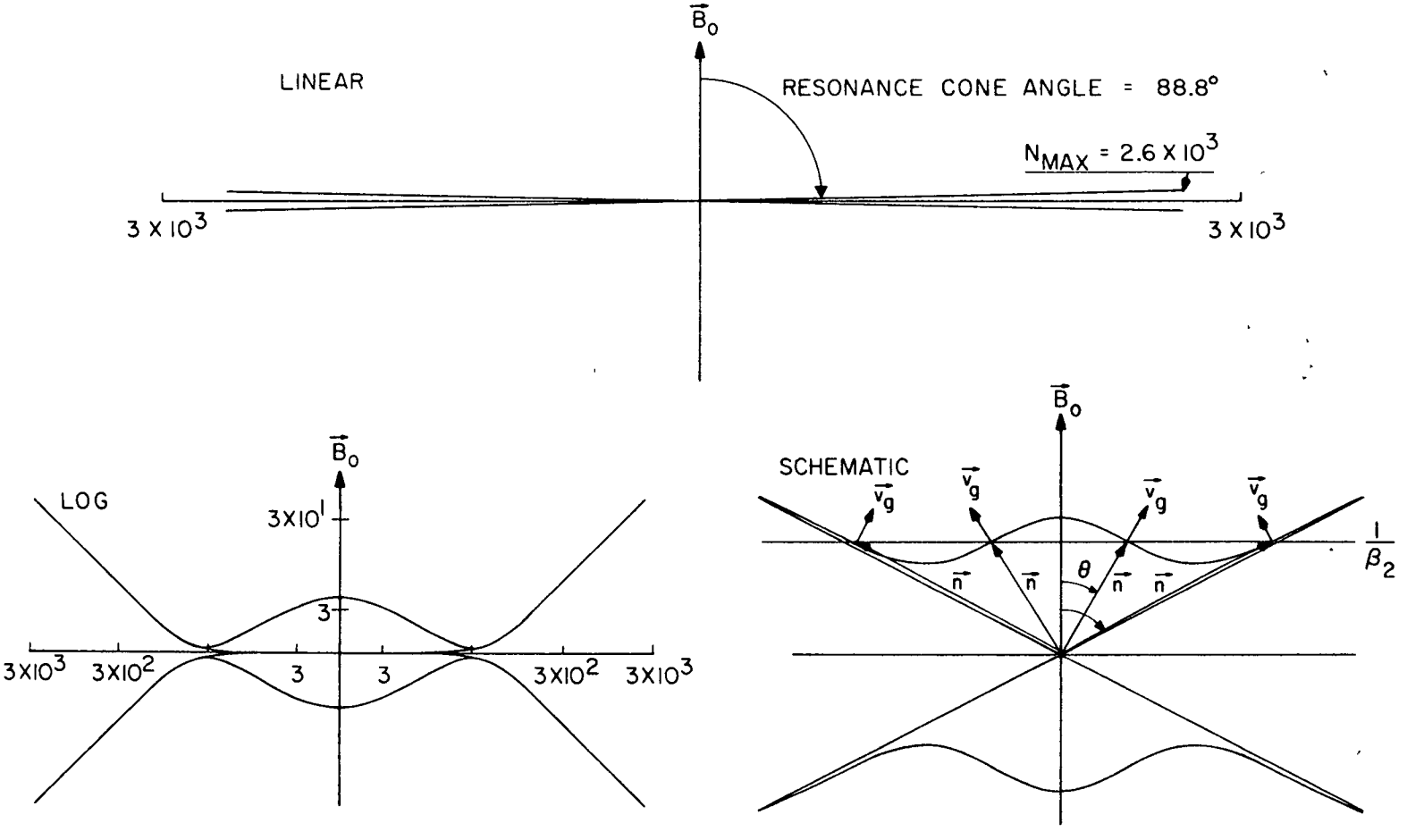

Figure 1

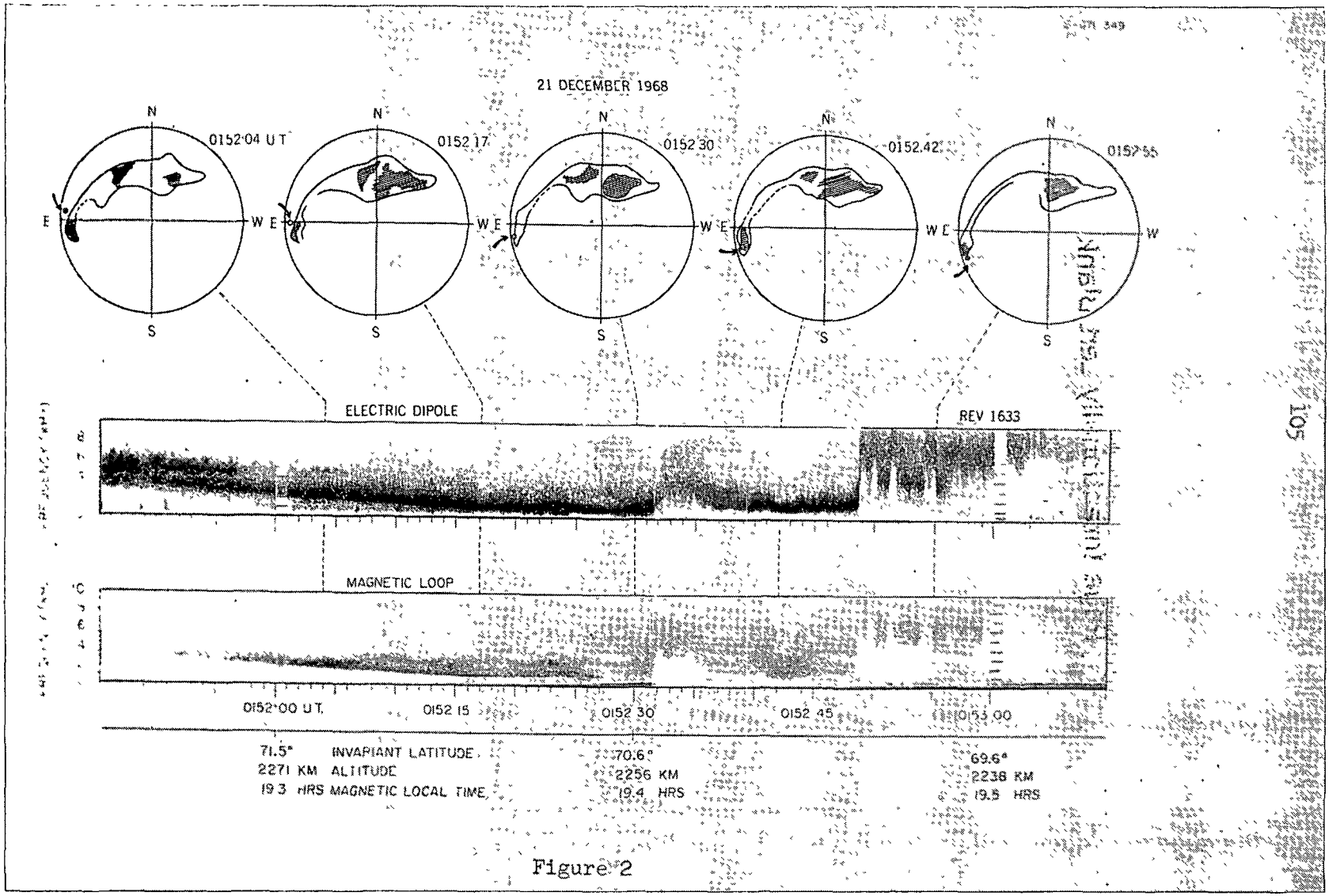
21 DECEMBER 1968
0152:04 U T
0152:17
0152:30
0152:42
0152:55
N
S
E
W
ELECTRIC DIPOLE
REV 1633
MAGNETIC LOOP
0152:00 U.T.
0152:15
0152:30
0152:45
0153:00
71.5° INVARIANT LATITUDE
2271 KM ALTITUDE
19.3 HRS MAGNETIC LOCAL TIME
70.6°
2256 KM
19.4 HRS
69.6°
2238 KM
19.5 HRS

Figure 2

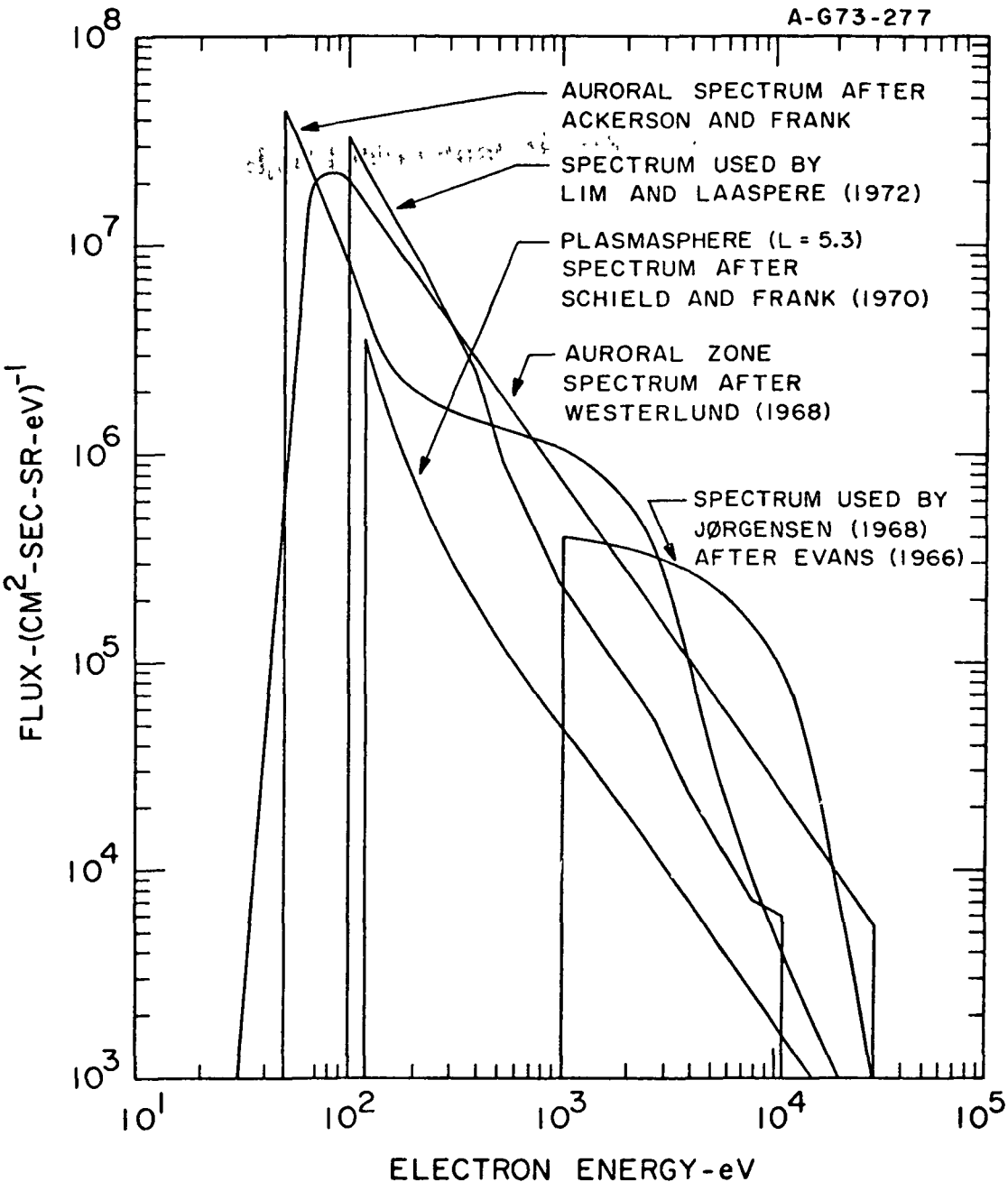
A-G73-277
AURORAL SPECTRUM AFTER ACKERSON AND FRANK
SPECTRUM USED BY LIM AND LAASPERE (1972)
PLASMASPHERE (L = 5.3) SPECTRUM AFTER SCHIELD AND FRANK (1970)
AURORAL ZONE SPECTRUM AFTER WESTERLUND (1968)
SPECTRUM USED BY JØRGENSEN (1968) AFTER EVANS (1966)
FLUX-(CM2-SEC-SR-eV)-1
ELECTRON ENERGY-eV
10^8
10^7
10^6
10^5
10^4
10^3
10^1
10^2
10^3
10^4
10^5

Figure 3

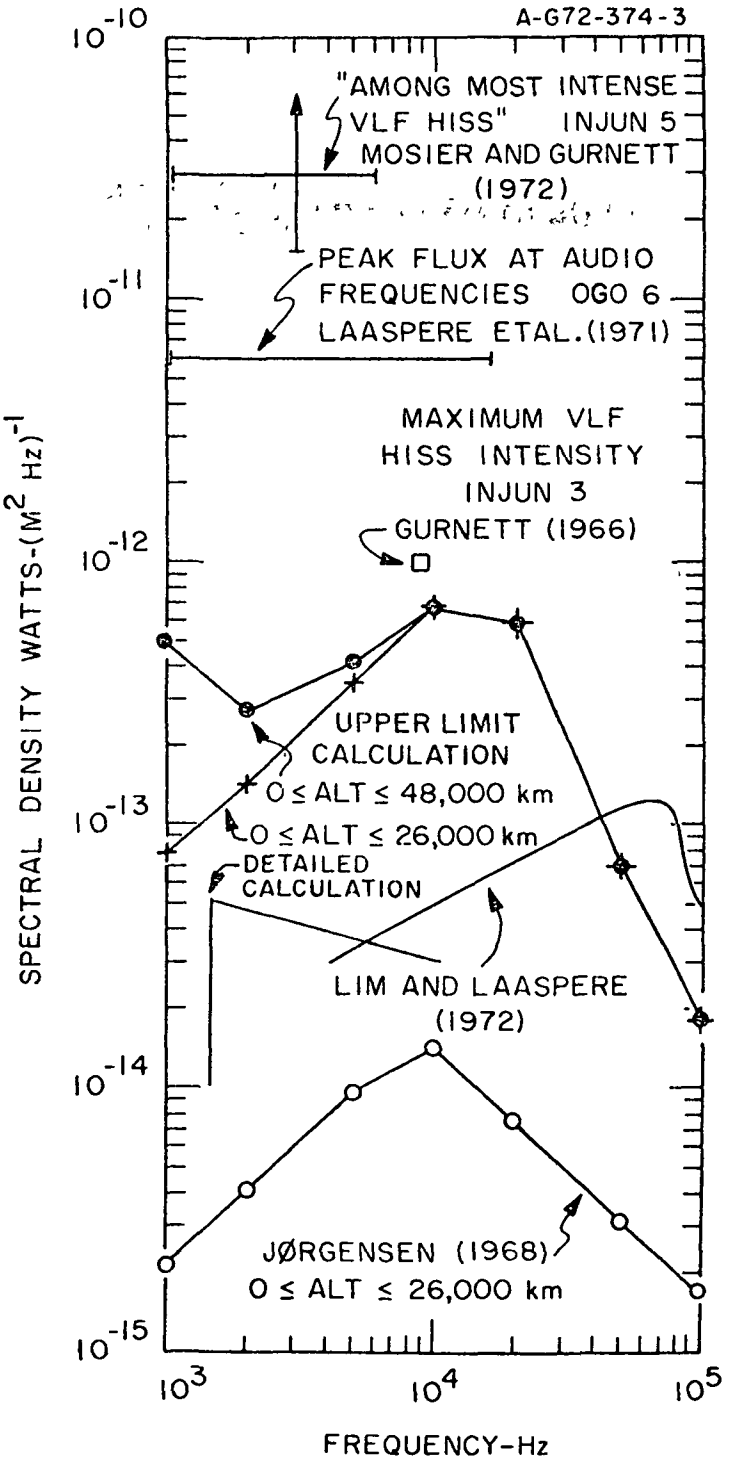
A-G72-374-3
"AMONG MOST INTENSE VLF HISS" INJUN 5 MOSIER AND GURNETT (1972)
PEAK FLUX AT AUDIO FREQUENCIES OGO 6 LAASPERE ETAL.(1971)
MAXIMUM VLF HISS INTENSITY INJUN 3 GURNETT (1966)
UPPER LIMIT CALCULATION
0 ≤ ALT ≤ 48,000 km
0 ≤ ALT ≤ 26,000 km
DETAILED CALCULATION
LIM AND LAASPERE (1972)
JØRGENSEN (1968)
0 ≤ ALT ≤ 26,000 km
SPECTRAL DENSITY WATTS-(M2 Hz)-1
FREQUENCY-Hz
10-10
10-11
10-12
10-13
10-14
10-15
10³
10⁴
10⁵

Figure 4

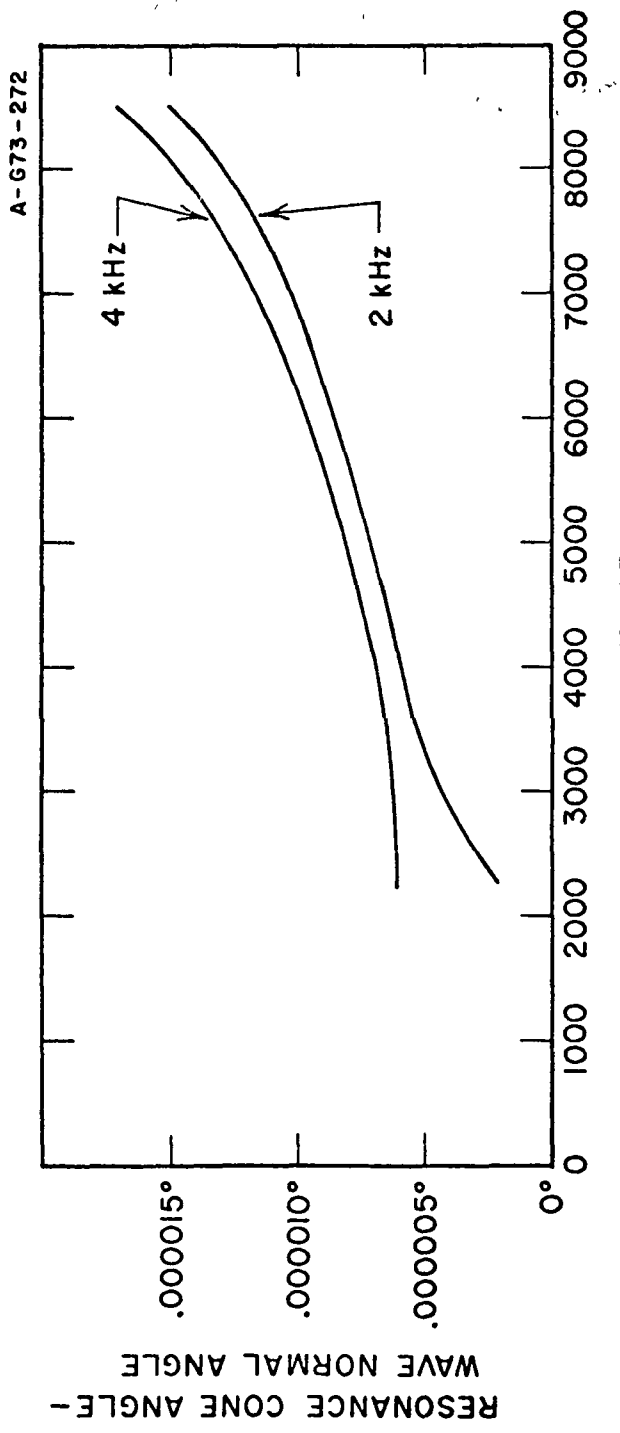
A-G73-272
4 kHz
2 kHz
0
1000
2000
3000
4000
5000
6000
7000
8000
9000
ALTITUDE - km
0°
.000005°
.000010°
.000015°
RESONANCE CONE ANGLE -
WAVE NORMAL ANGLE

Figure 5

A-G73-271

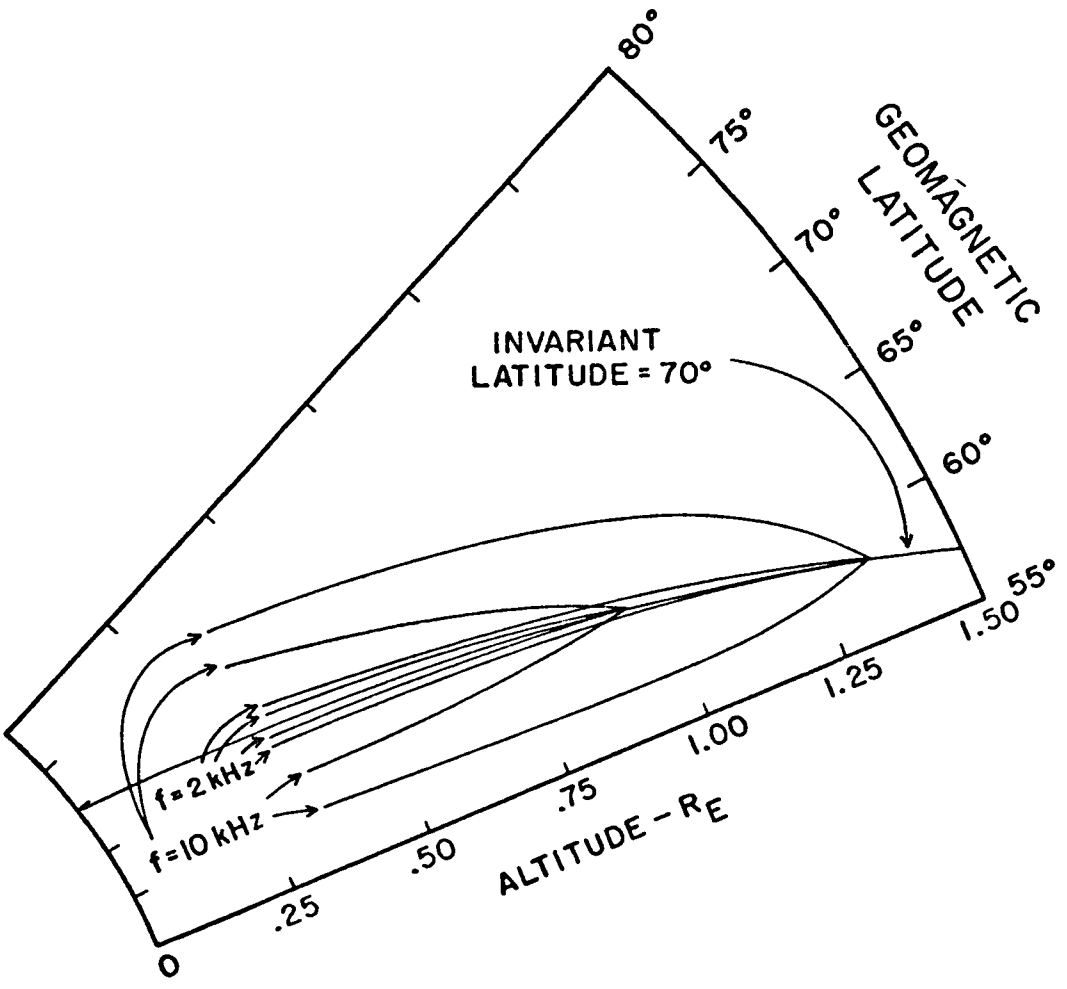

Figure 6

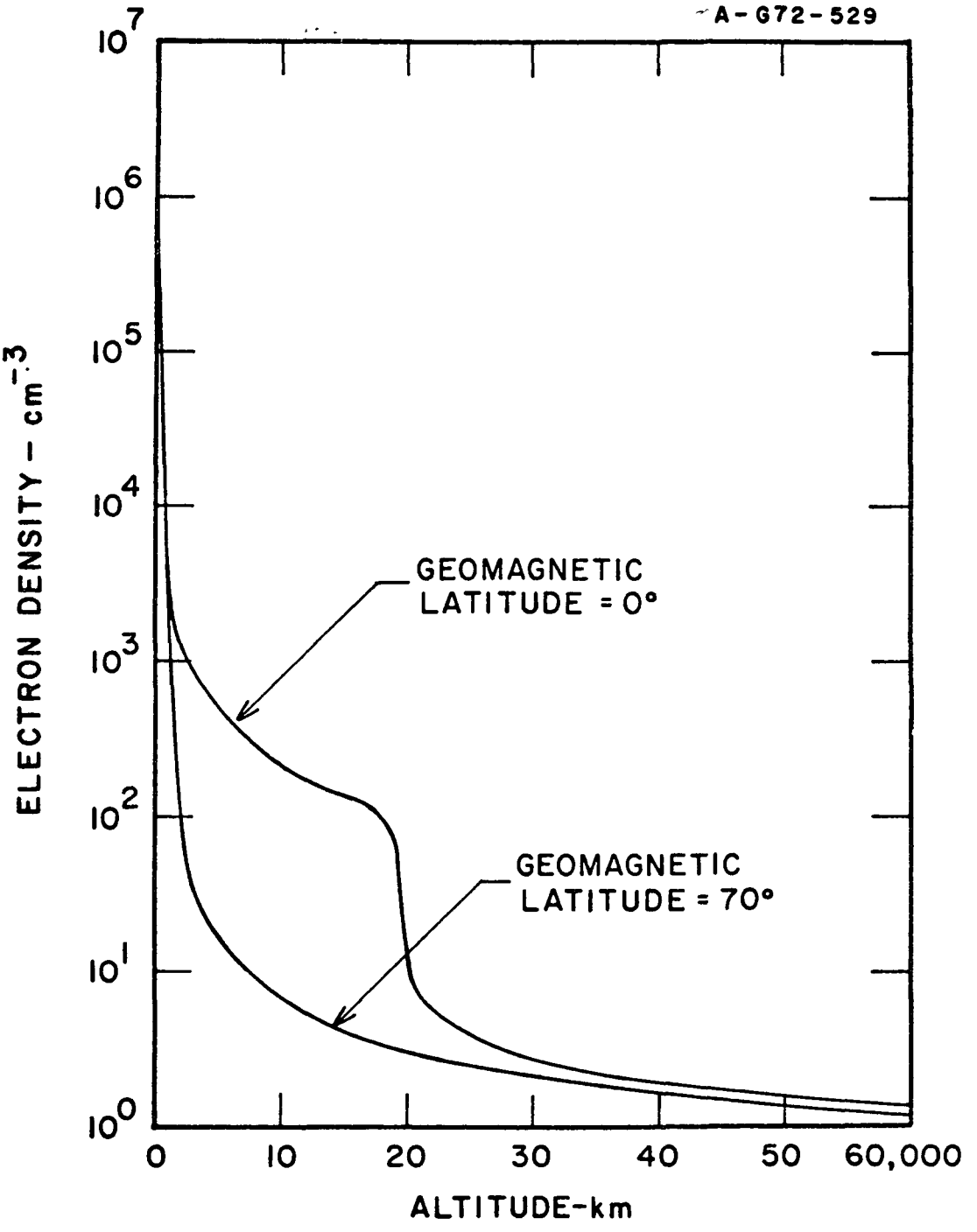
A-G72-529
ELECTRON DENSITY - cm⁻³
10⁷
10⁶
10⁵
10⁴
10³
10²
10¹
10⁰
GEOMAGNETIC LATITUDE = 0°
GEOMAGNETIC LATITUDE = 70°
0
10
20
30
40
50
60,000
ALTITUDE-km

Figure 7

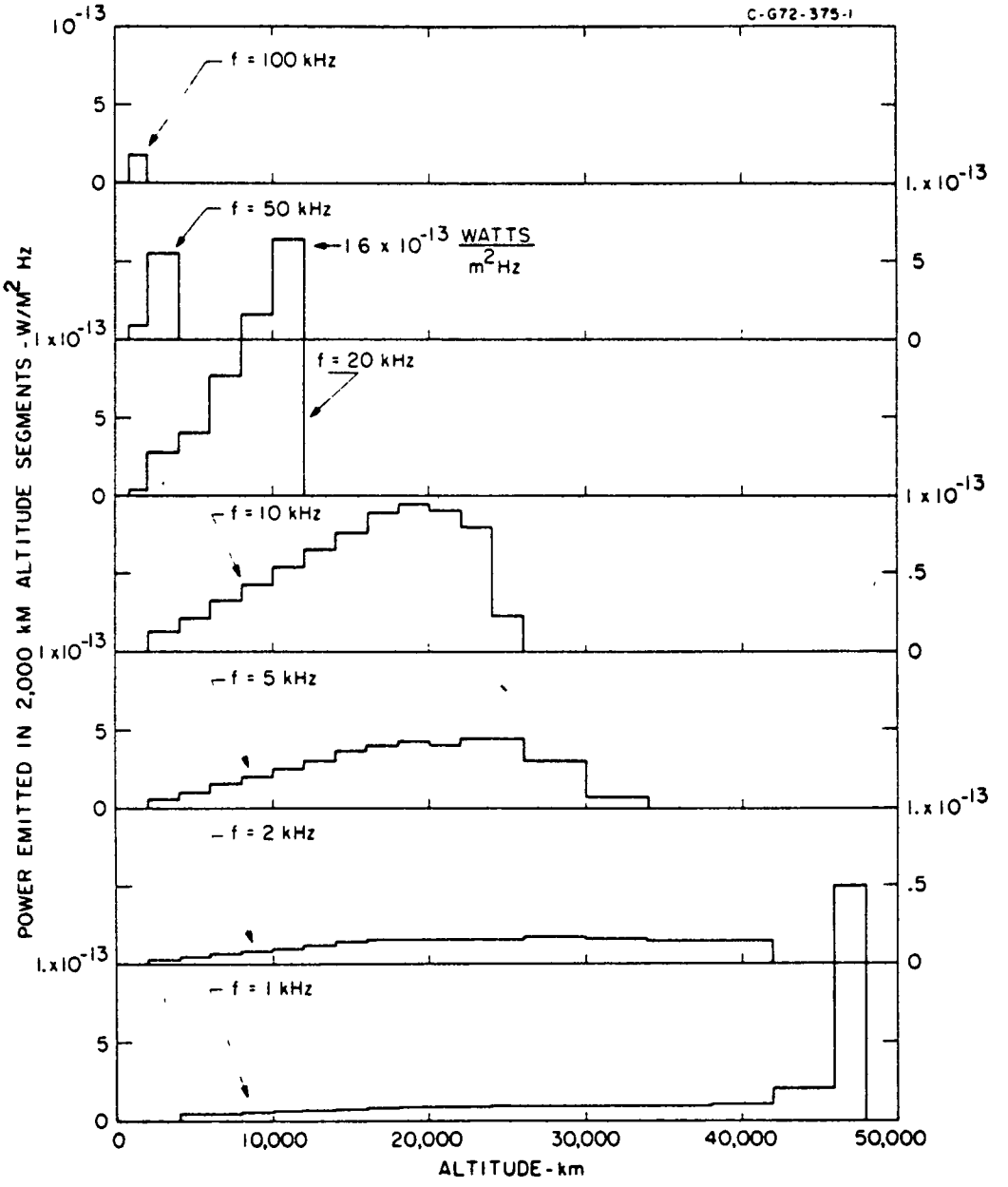
C-G72-375-1
f = 100 kHz
f = 50 kHz
16 x 10^-13 WATTS / m^2 Hz
f = 20 kHz
f = 10 kHz
f = 5 kHz
f = 2 kHz
f = 1 kHz
POWER EMITTED IN 2,000 kM ALTITUDE SEGMENTS - W/M^2 Hz
ALTITUDE - km
0
10,000
20,000
30,000
40,000
50,000

Figure 8

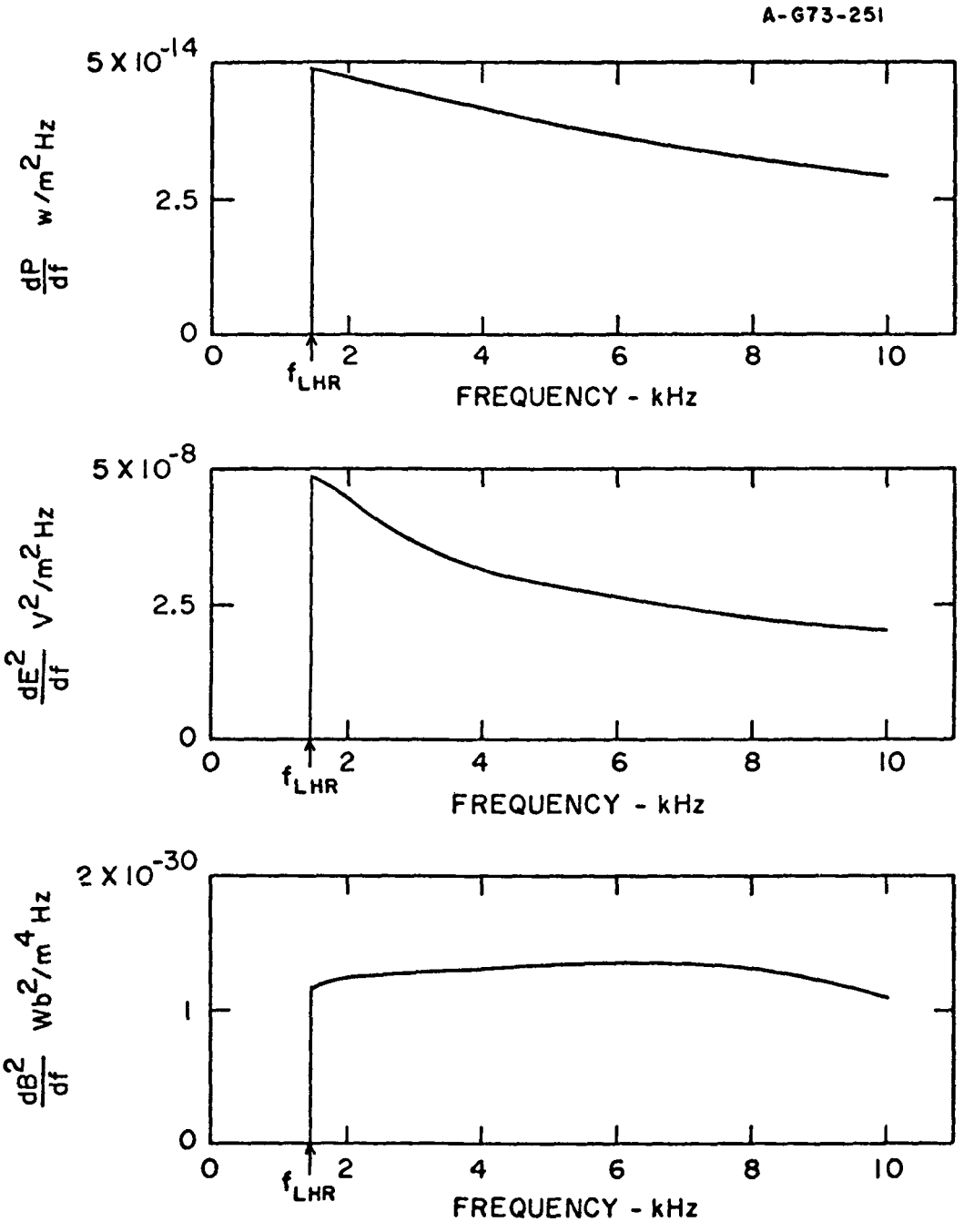
A-G73-251
5 X 10^-14
2.5
0
dP/df w/m^2Hz
0
2
4
6
8
10
f_LHR
FREQUENCY - kHz
5 X 10^-8
2.5
0
dE^2/df V^2/m^2Hz
0
2
4
6
8
10
f_LHR
FREQUENCY - kHz
2 X 10^-30
1
0
dB^2/df Wb^2/m^4Hz
0
2
4
6
8
10
f_LHR
FREQUENCY - kHz

Figure 9

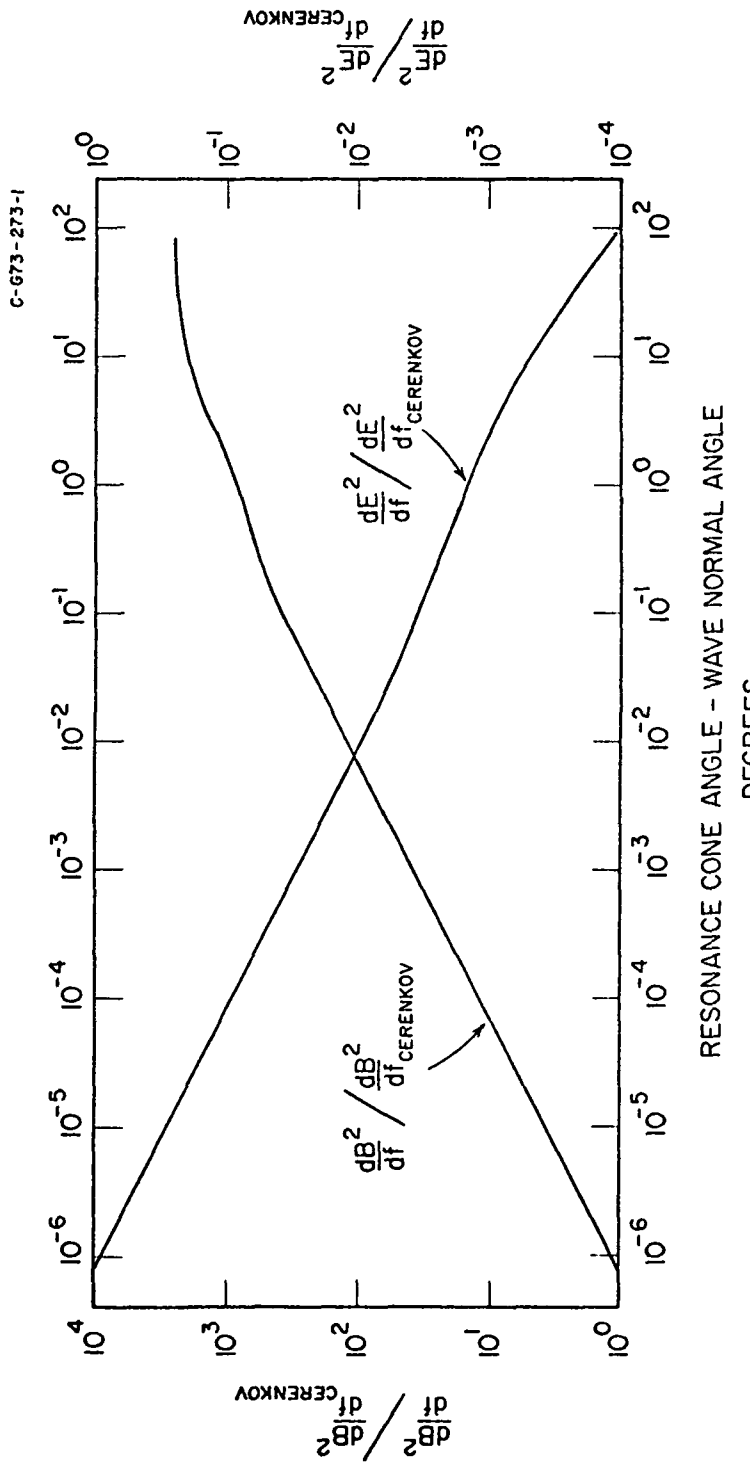
C-673-273-1
$\frac{dB^2}{df} / \frac{dB^2}{df}_{CERENKOV}$
$\frac{dE^2}{df} / \frac{dE^2}{df}_{CERENKOV}$
$\frac{dB^2}{df} / \frac{dB^2}{df}_{CERENKOV}$
$\frac{dE^2}{df} / \frac{dE^2}{df}_{CERENKOV}$
RESONANCE CONE ANGLE - WAVE NORMAL ANGLE
DEGREES

Figure 10

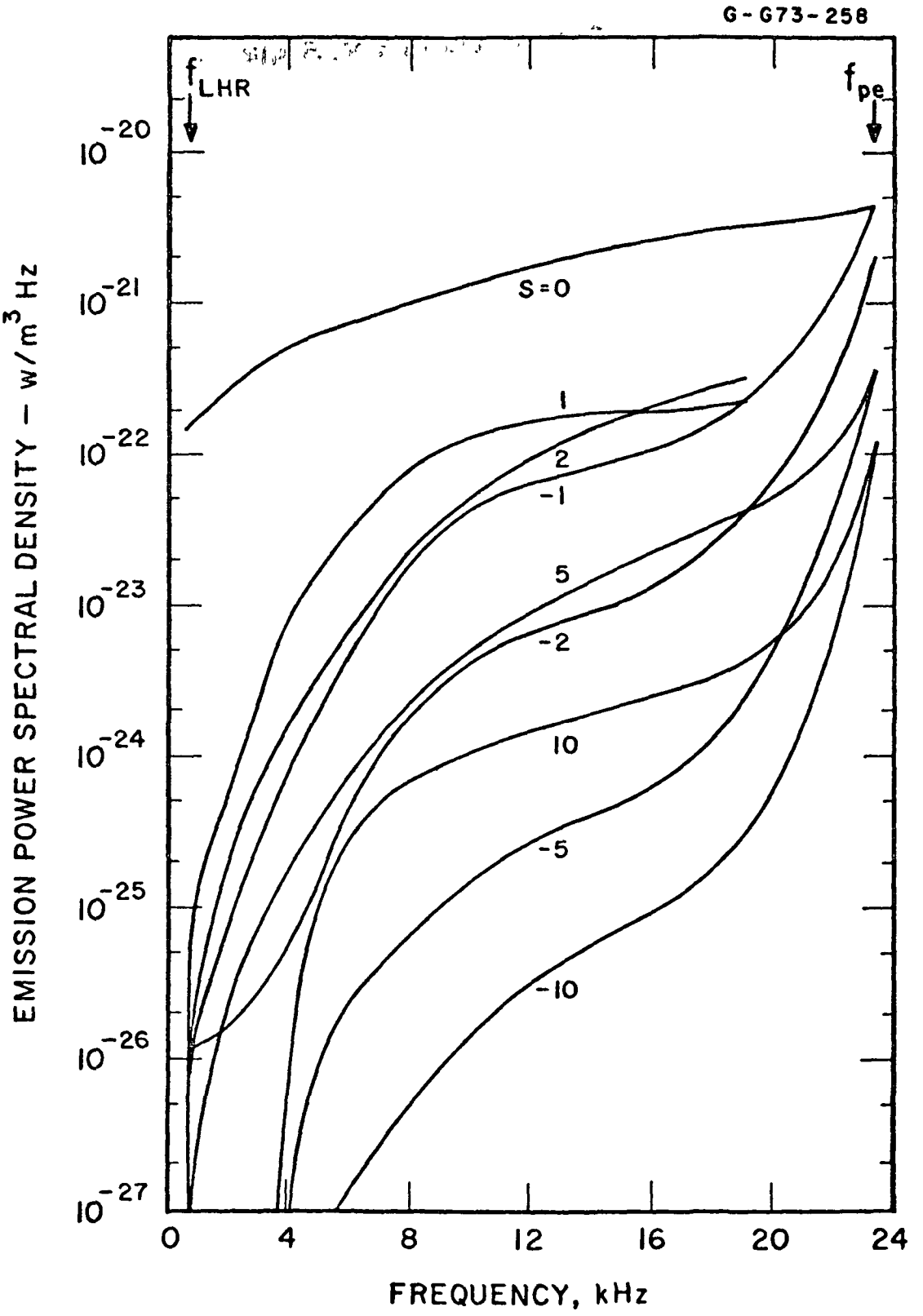
G-G73-258
f_{LHR}
f_{pe}
10^{-20}
10^{-21}
10^{-22}
10^{-23}
10^{-24}
10^{-25}
10^{-26}
10^{-27}
S=0
1
2
-1
5
-2
10
-5
-10
0
4
8
12
16
20
24
EMISSION POWER SPECTRAL DENSITY – w/m^3 Hz
FREQUENCY, kHz

Figure 11

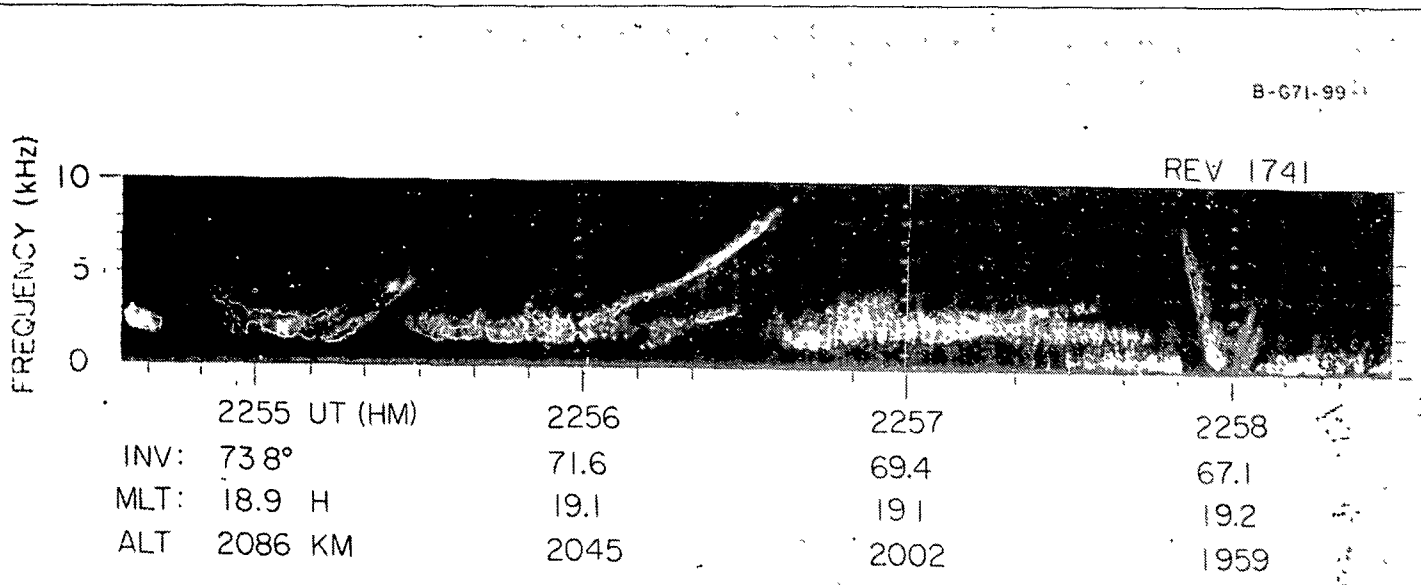
B-671-99
REV 1741
FREQUENCY (kHz)
10
5
0
2255 UT (HM)
2256
2257
2258
INV: 73 8°
71.6
69.4
67.1
MLT: 18.9 H
19.1
19 1
19.2
ALT 2086 KM
2045
2002
1959

Figure 12

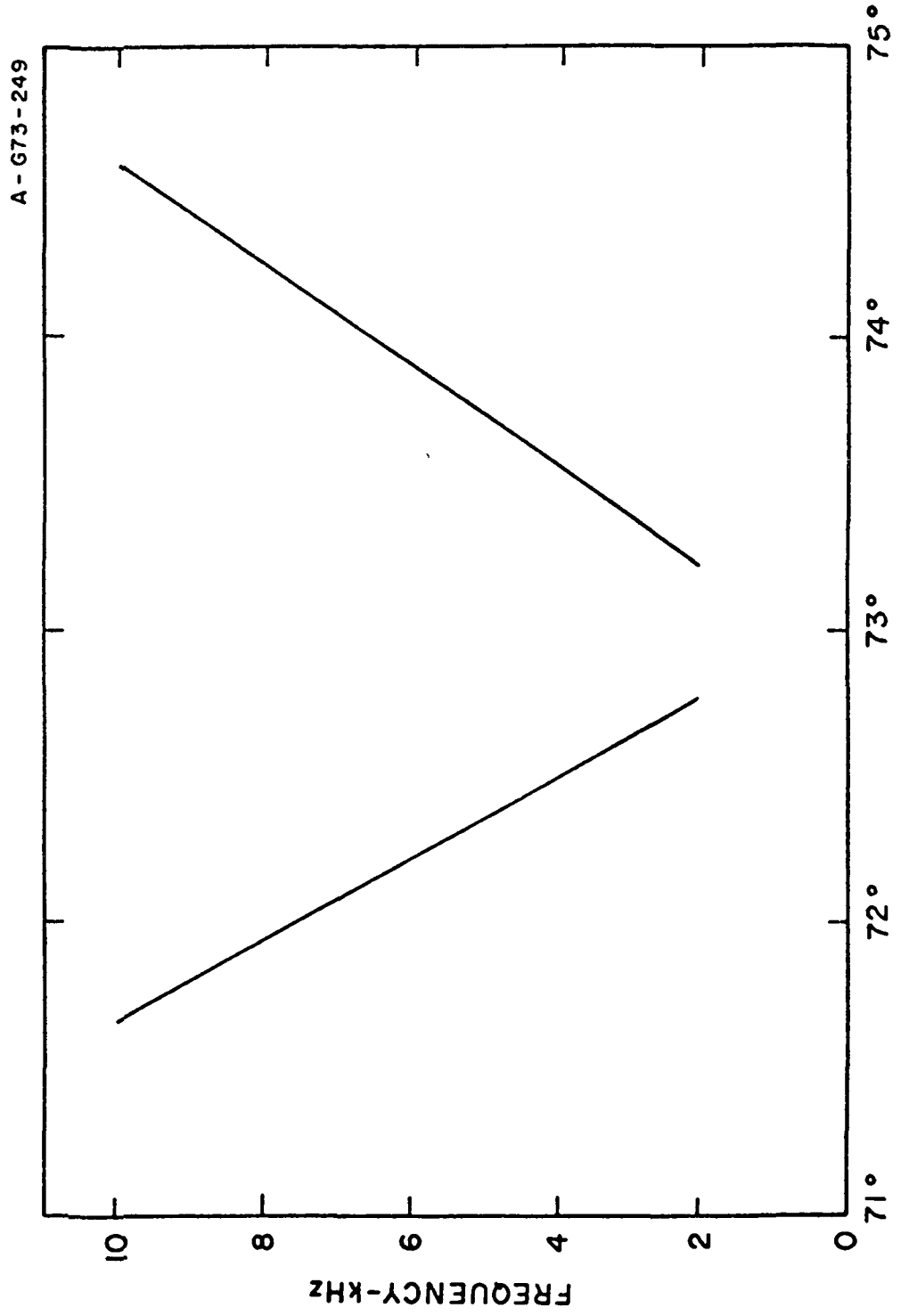
A-673-249
FREQUENCY-kHz
0
2
4
6
8
10
71°
72°
73°
74°
75°
INVARIANT LATITUDE

Figure 13

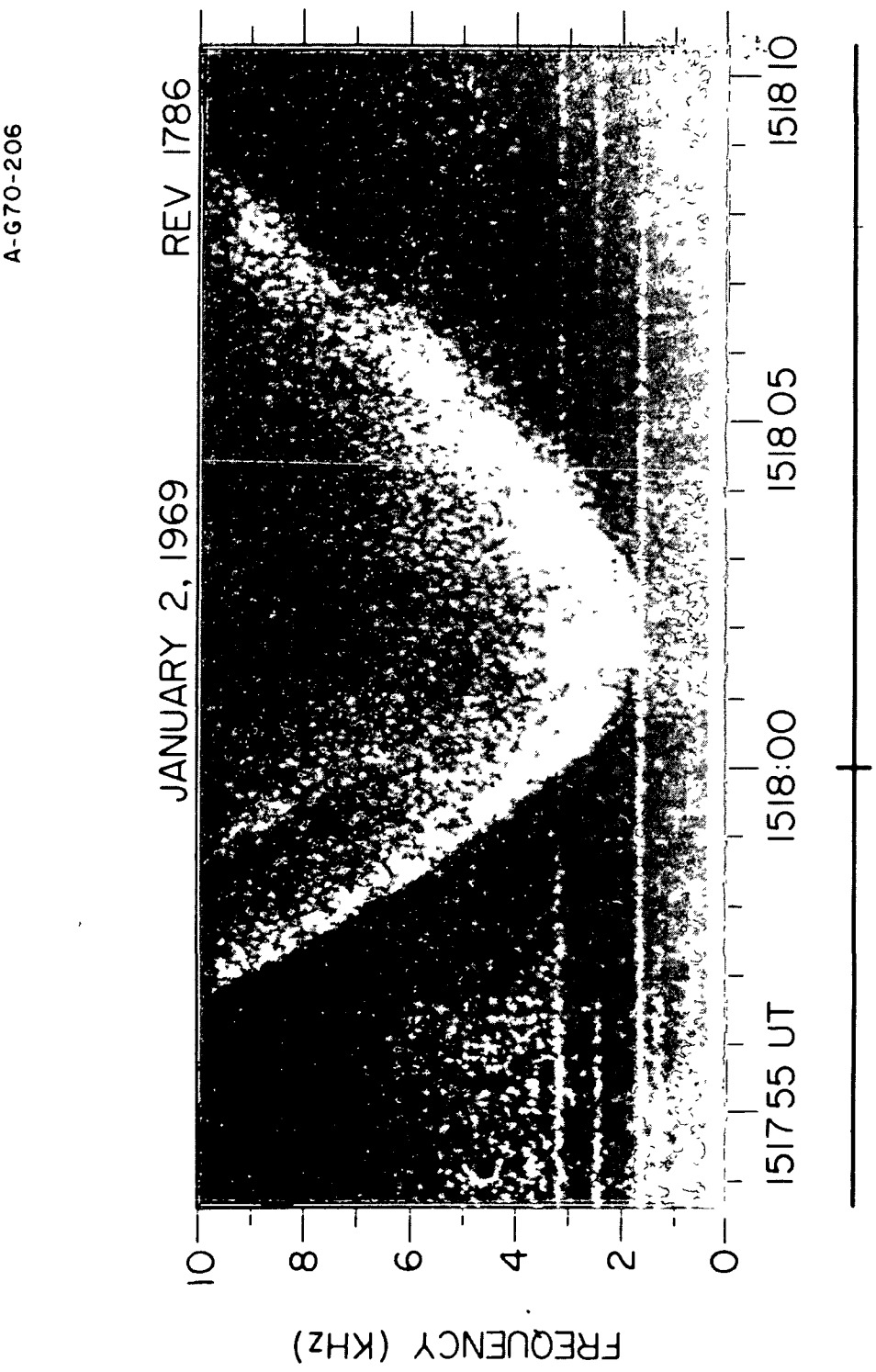
A-G70-206
JANUARY 2, 1969
REV 1786
FREQUENCY (KHz)
10
8
6
4
2
0
1517 55 UT
1518:00
1518 05
1518 10
MLT: 7 78 HR
INV: 69.5°
ALT: 2539 KM

Figure 14

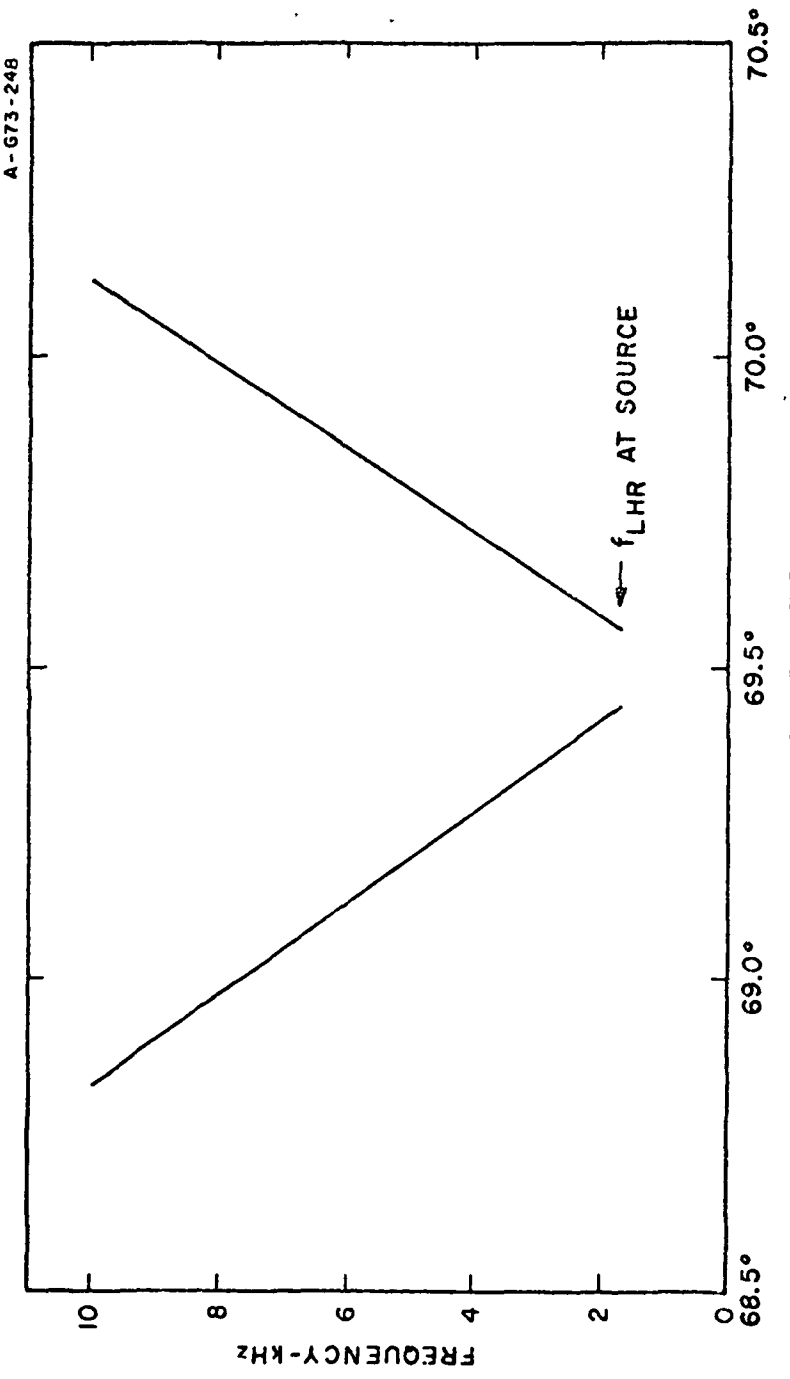
A-G73-248
FREQUENCY-kHz
0
2
4
6
8
10
68.5°
69.0°
69.5°
70.0°
70.5°
INVARIANT LATITUDE
f_{LHR} AT SOURCE

Figure 15

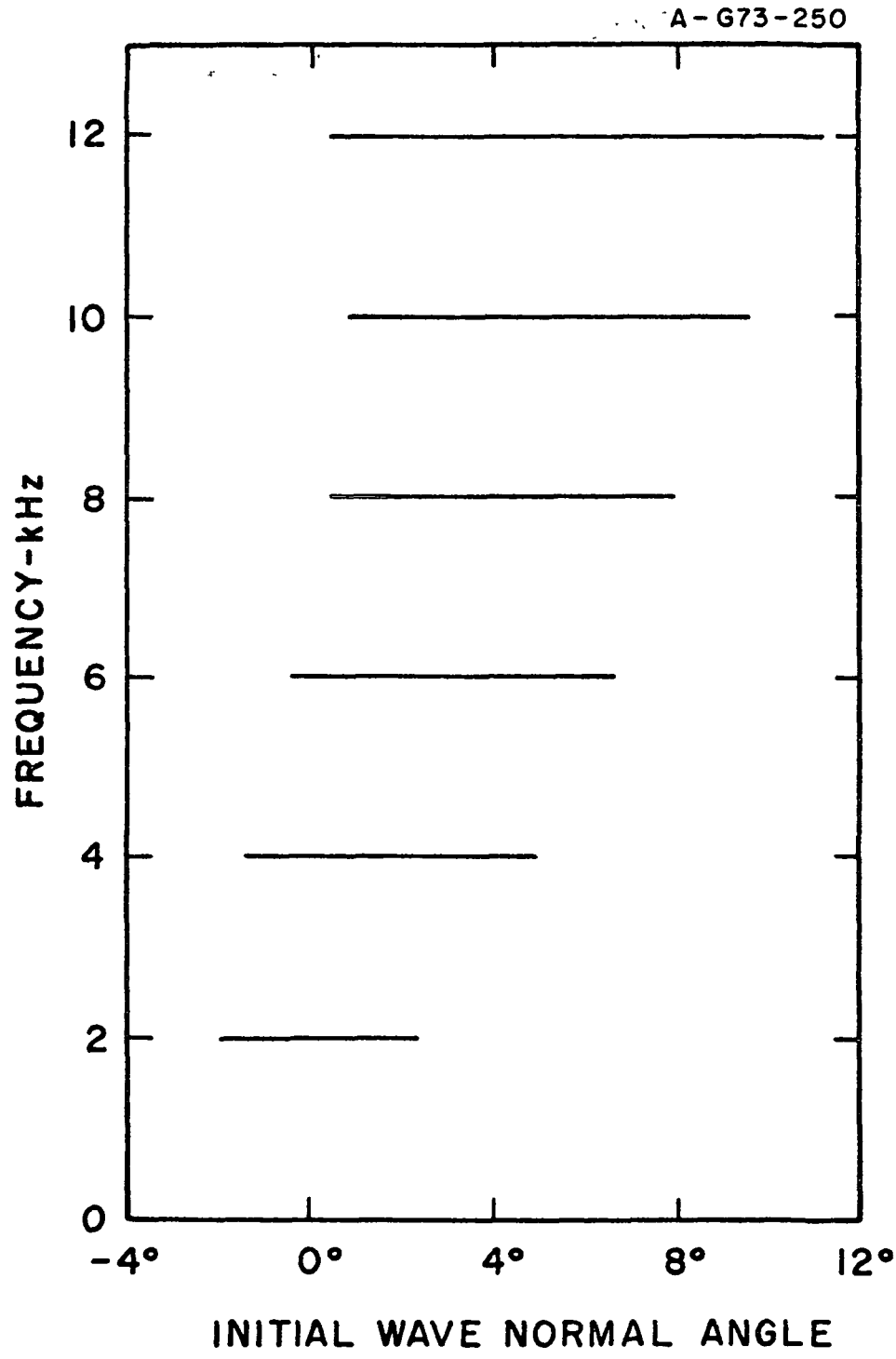
A-G73-250
12
10
8
6
4
2
0
FREQUENCY-kHz
-4°
0°
4°
8°
12°
INITIAL WAVE NORMAL ANGLE

Figure 16

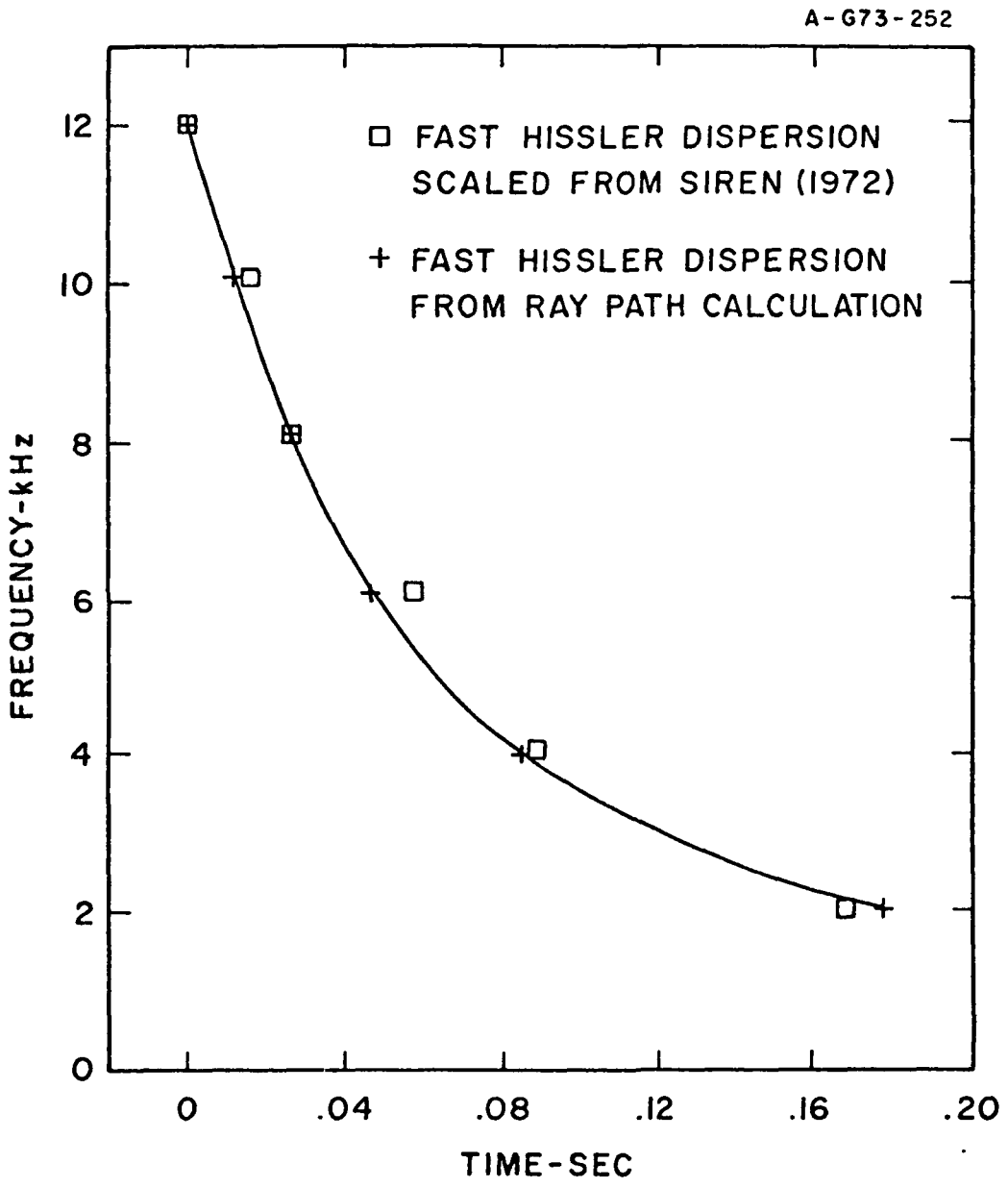
A-G73-252
FAST HISSLER DISPERSION SCALED FROM SIREN (1972)
+ FAST HISSLER DISPERSION FROM RAY PATH CALCULATION
FREQUENCY-kHz
TIME-SEC
0
2
4
6
8
10
12
0
.04
.08
.12
.16
.20

Figure 17

A-G73-265

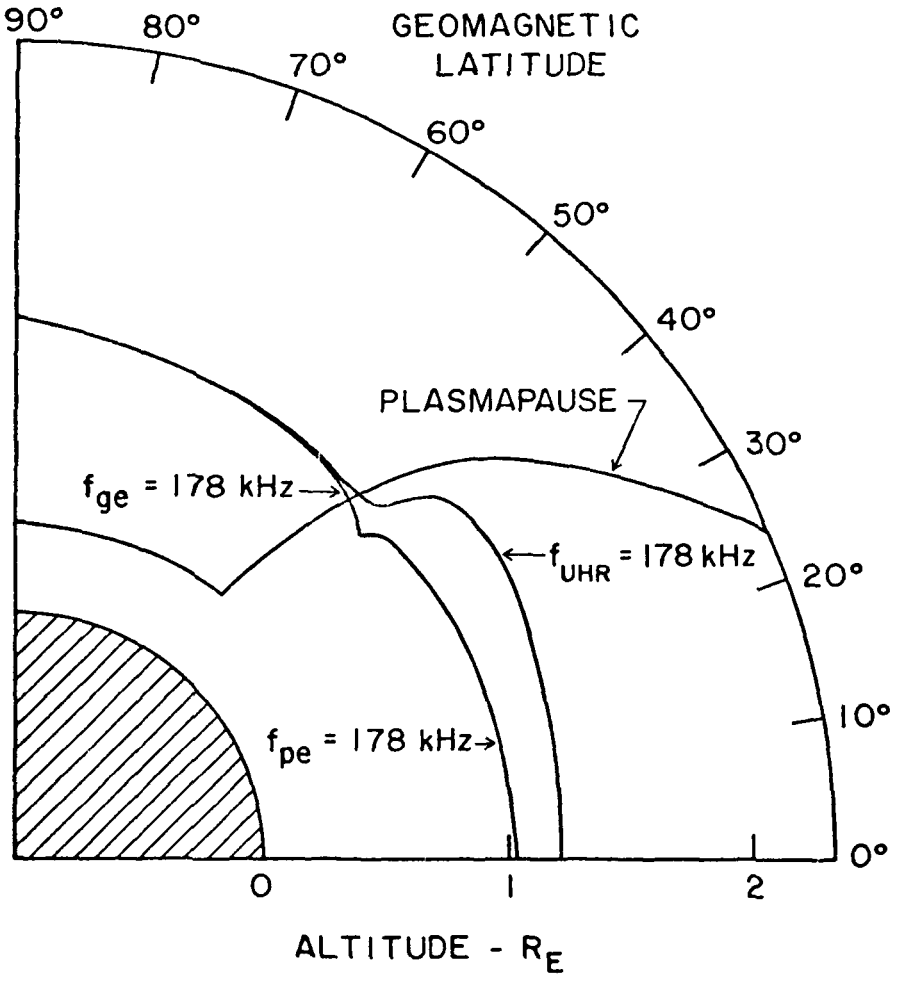

Figure 18

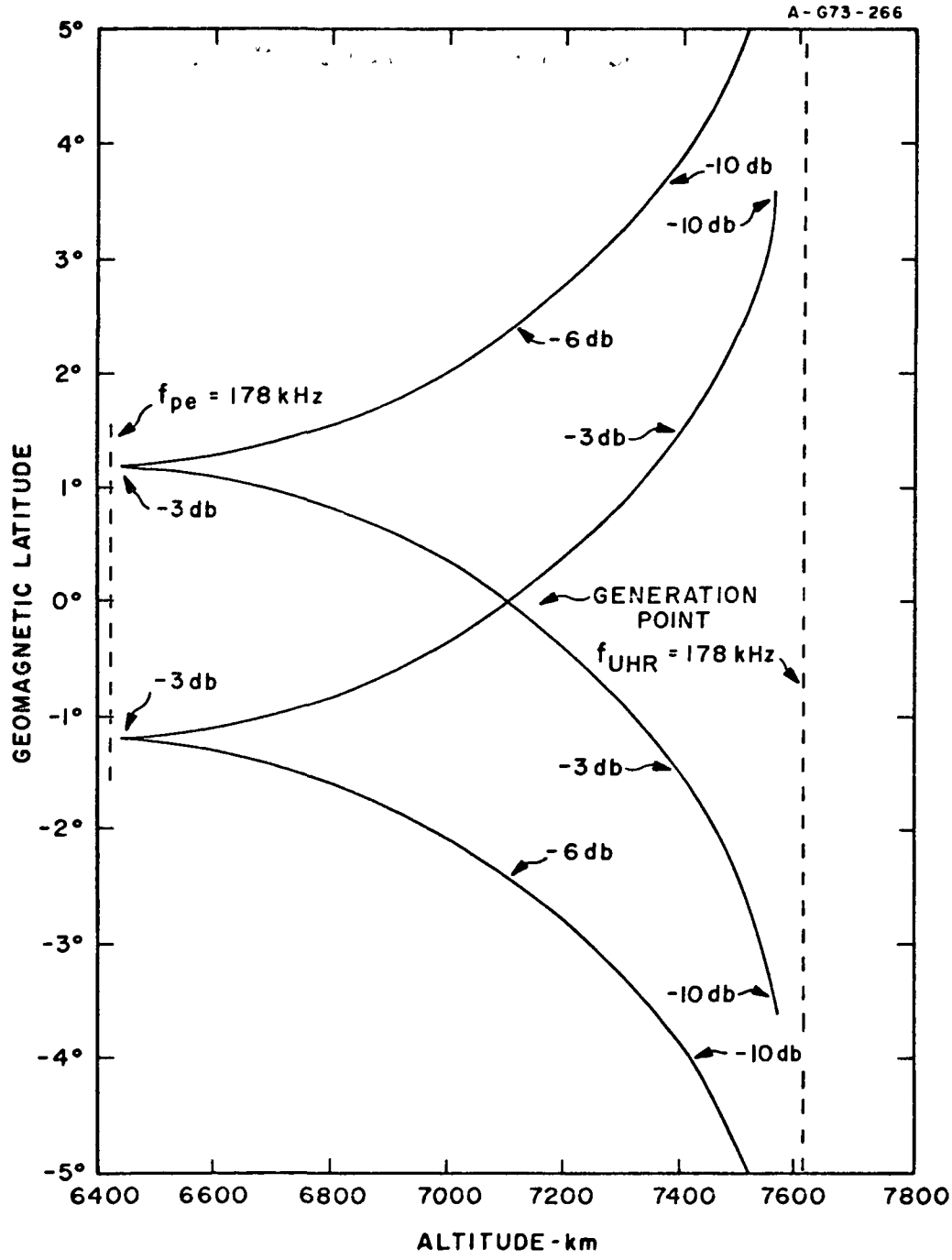
A-G73-266
5°
4°
3°
2°
1°
0°
-1°
-2°
-3°
-4°
-5°
GEOMAGNETIC LATITUDE
6400
6600
6800
7000
7200
7400
7600
7800
ALTITUDE-km
-10 db
-10 db
-6 db
f_{pe} = 178 kHz
-3 db
-3 db
GENERATION POINT
f_{UHR} = 178 kHz
-3 db
-3 db
-6 db
-10 db
-10 db

Figure 19

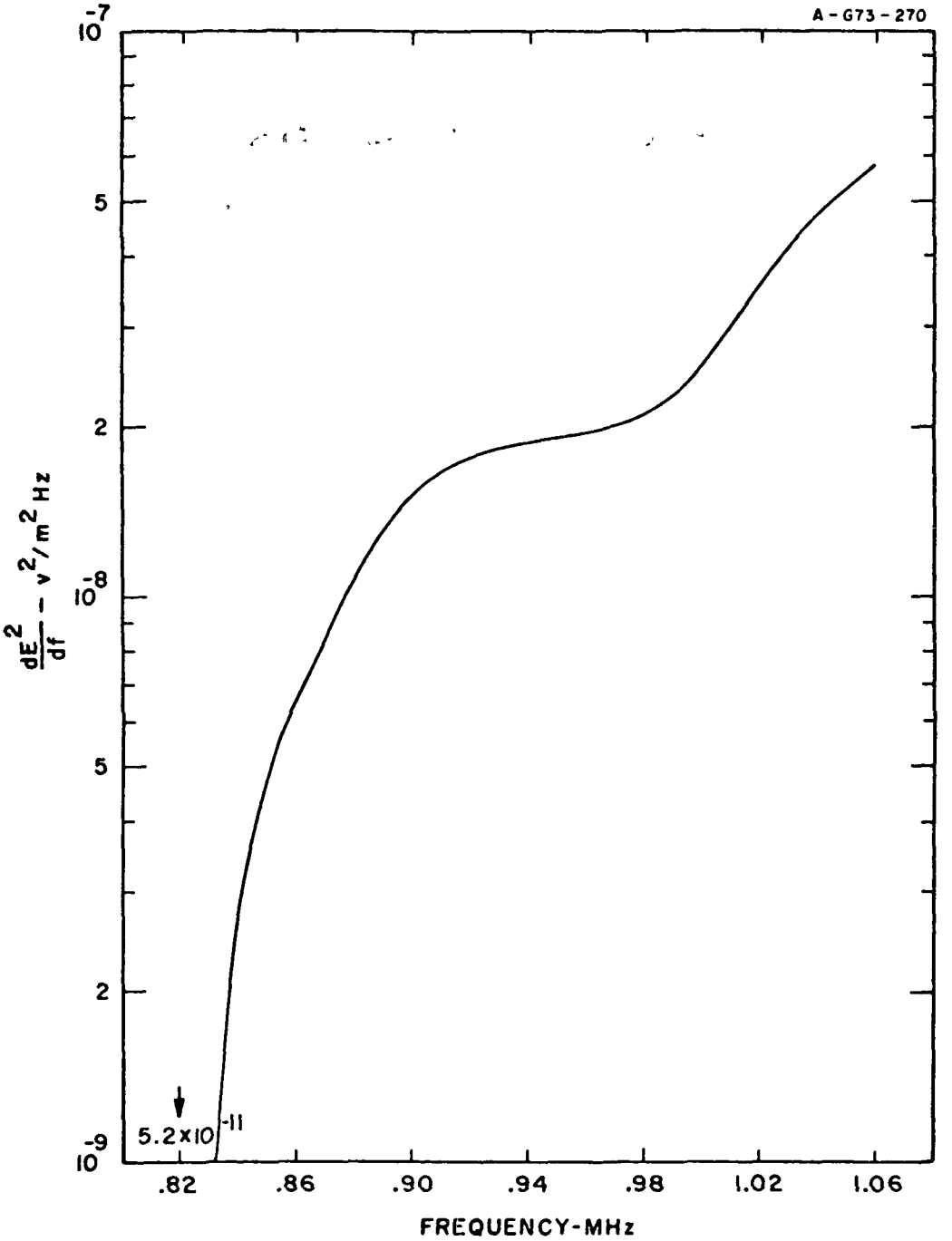
A-G73-270
10^{-7}
5
2
10^{-8}
5
2
10^{-9}
$\frac{dE^2}{df}$ - v^2/m^2 Hz
5.2x10^{-11}
.82
.86
.90
.94
.98
1.02
1.06
FREQUENCY-MHz

Figure 20

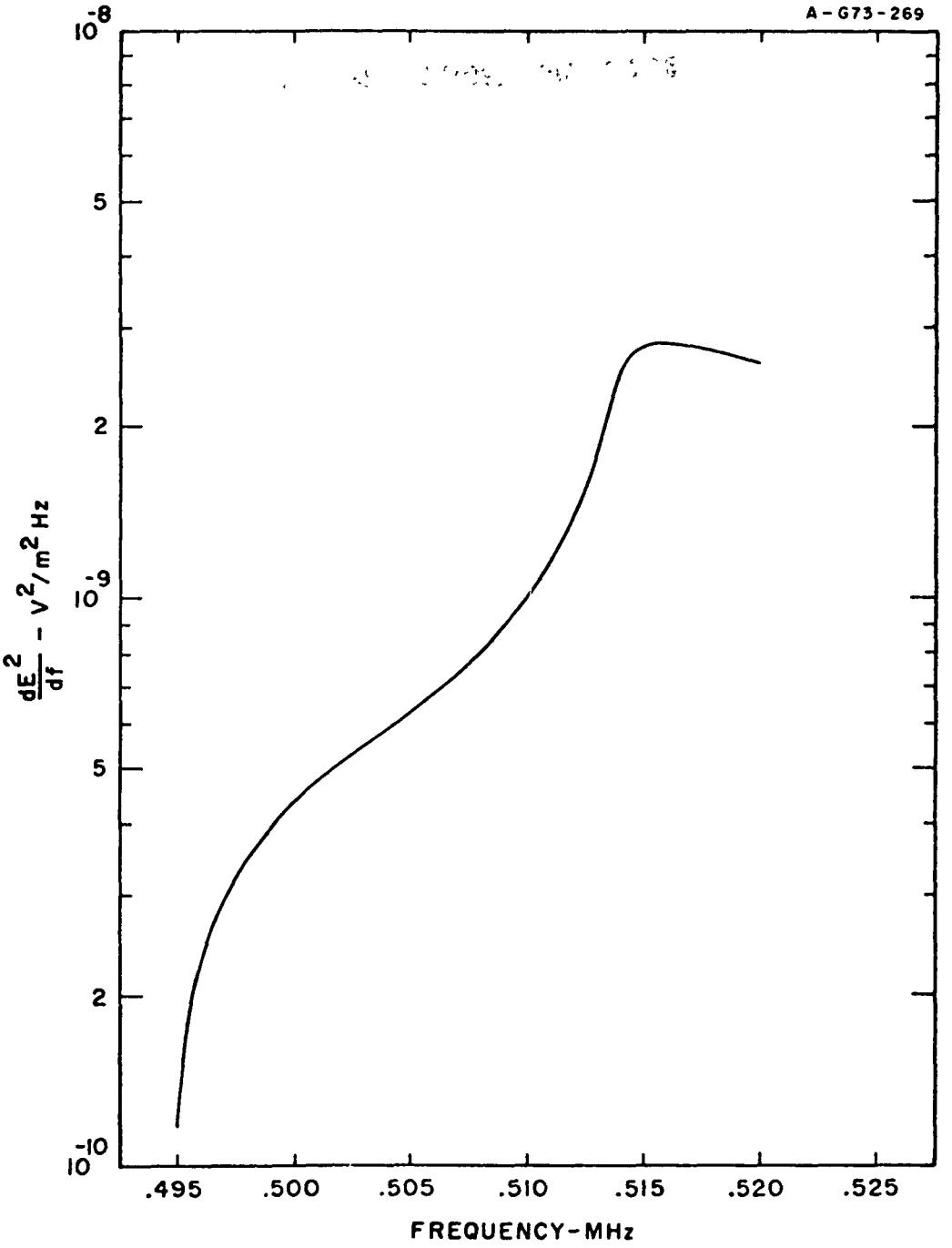
A-G73-269
10^{-8}
5
2
10^{-9}
5
2
10^{-10}
$\frac{dE^2}{df}$ - V^2/m^2 Hz
.495
.500
.505
.510
.515
.520
.525
FREQUENCY-MHz

Figure 21

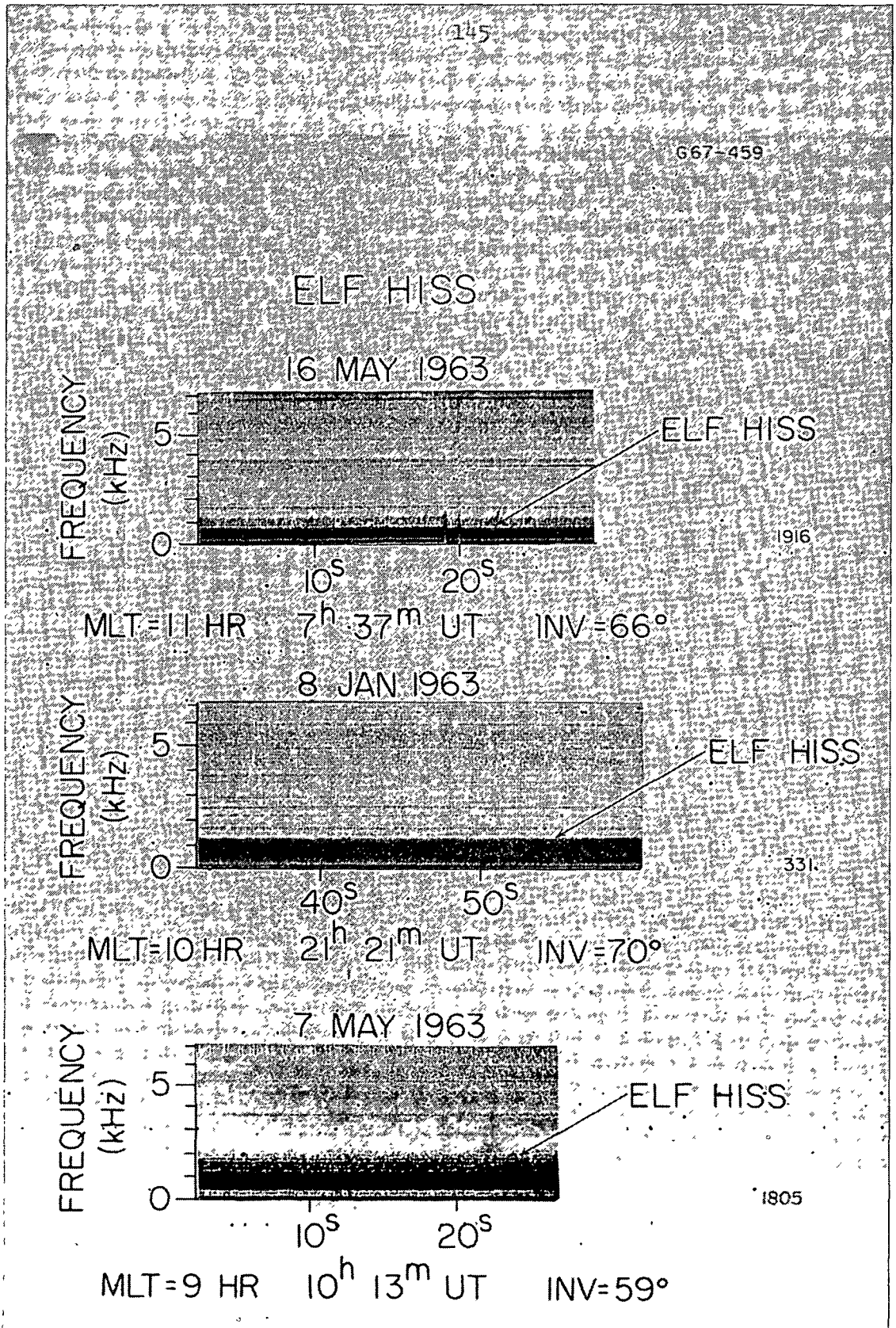
G67-459
ELF HISS
16 MAY 1963
FREQUENCY (kHz)
5
0
ELF HISS
1916
10s
20s
MLT=11 HR
7h 37m UT
INV=66°
8 JAN 1963
FREQUENCY (kHz)
5
0
ELF HISS
331
40s
50s
MLT=10 HR
21h 21m UT
INV=70°
7 MAY 1963
FREQUENCY (kHz)
5
0
ELF HISS
1805
10s
20s
MLT=9 HR
10h 13m UT
INV=59°

Figure 22